

000 001 002 003 004 005 U2-BENCH: BENCHMARKING LARGE VISION-LANGUAGE 006 MODELS ON ULTRASOUND UNDERSTANDING 007 008 009 010

005 **Anonymous authors**

006 Paper under double-blind review
007
008
009
010

ABSTRACT

011 Ultrasound is a widely-used imaging modality critical to global healthcare, yet its interpreta-
012 tion remains challenging due to variability in image quality caused by operator dependency,
013 noise, and anatomical complexity. Although large vision-language models (LVLMs) have
014 demonstrated impressive multimodal capabilities across natural and medical domains, their
015 performance on ultrasound remains largely unexplored. We introduce U2-BENCH, the
016 first comprehensive benchmark to evaluate LVLMs on ultrasound understanding across
017 classification, detection, regression, and text generation tasks. U2-BENCH aggregates
018 7,241 cases spanning 15 anatomical regions and defines 8 clinically inspired tasks, such
019 as *diagnosis*, *view recognition*, *lesion localization*, *clinical value estimation*, and *report*
020 *generation*, across 50 ultrasound application scenarios. We evaluate 23 state-of-the-art
021 LVLMs, both open- and closed-source, general-purpose and medical-specific. Our results
022 reveal strong performance on image-level classification, but persistent challenges in spatial
023 reasoning and clinical language generation. U2-BENCH establishes a rigorous and unified
024 testbed to assess and accelerate LVLM research in the uniquely multimodal domain of
025 medical ultrasound imaging.¹
026

027 1 INTRODUCTION

029 Ultrasound (US) is one of the most widely used imaging modalities in global healthcare — essential in
030 obstetrics, emergency medicine, cardiology, and low-resource settings — while its interpretation remains
031 notoriously difficult (Hewson & Bedforth, 2023). Compared to modalities such as computed tomography (CT),
032 magnetic resonance imaging (MRI), positron emission tomography (PET), and whole-slide imaging (WSI),
033 which offer higher spatial resolution, consistent image quality, and standardized anatomical views, ultrasound
034 is real-time and low-cost but highly operator-dependent and frequently affected by imaging artifacts (Sharma
035 et al., 2021). In addition, in contrast to these modalities, US is dynamically presenting three-dimensional
036 (3D) anatomies in image sequences. Therefore, accurate interpretation of US demands not only visual pattern
037 recognition in the images, but also an understanding of anatomy and capturing of dynamic spatial-context
038 reasoning, typically requiring extensive prior domain expertise (Wang et al., 2022). These challenges have
039 limited the applicability of earlier artificial intelligence (AI) models. However, recent advances in medical
040 large vision-language models (LVLMs) have shown promise in overcoming these barriers (Chen et al., 2024b;
041 Xia et al., 2024; Huang et al., 2025), potentially offering a robust multimodal understanding of complex,
042 noisy, and context-rich ultrasound data.

043 While progress in medical LVLM has been rapid, most previous models and benchmarks focus on those less
044 noisy and static imaging modalities (Ji et al., 2022; Huang et al., 2023; Sivasubramaniam et al., 2024), leaving

045 ¹Codes are available at: <https://anonymous.4open.science/r/U2-Bench-F781/VLMEVALKIT/>

046 Data is available on HuggingFace.

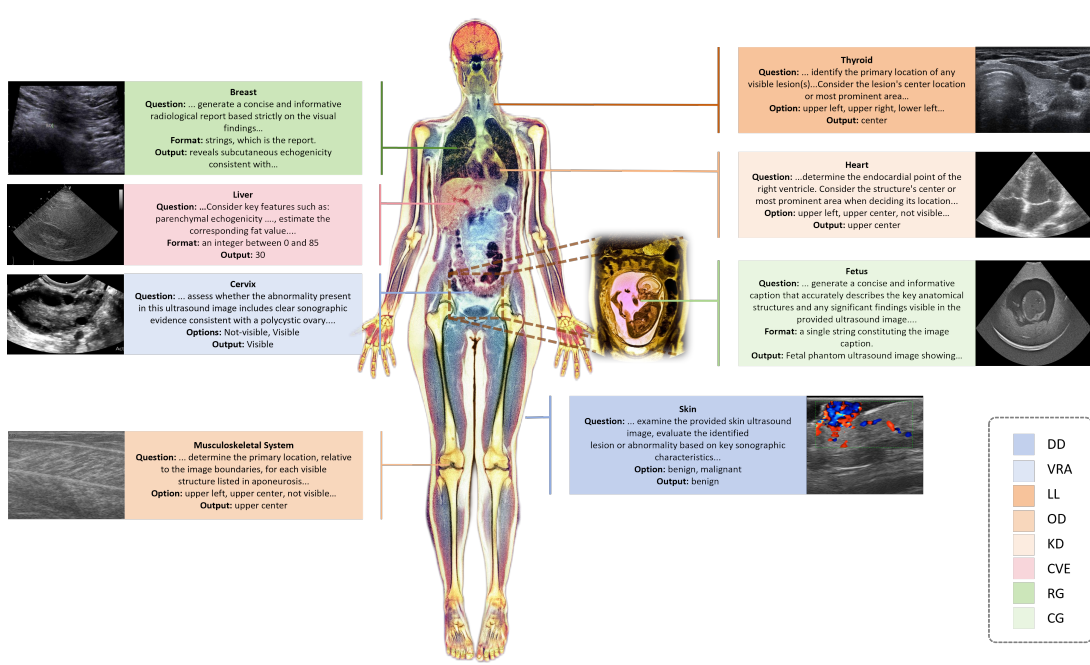


Figure 1: **Examples of the 8 benchmark tasks in U2-BENCH across diverse anatomical regions.** Each callout, consisting of the question prompt, expected output format, and sample output, highlights a representative ultrasound application scenario of the corresponding task. Tasks involve disease diagnosis (DD), view recognition and assessment (VRA), lesion localization (LL), organ detection (OD), keypoint detection (KD), clinical value estimation (CVE), report generation (RG) and caption generation (CG).

the complexities of ultrasound largely unaddressed. Prior efforts in ultrasound AI are typically based on small, task-specific datasets (Xiao et al., 2025), such as fetal plane identification (Guo et al., 2024) or pathology segmentation (Indelman et al., 2024; Ravishankar et al., 2023). As model capabilities grow, a public, balanced benchmark for ultrasound understanding is needed to evaluate whether emerging LVLMs can generalize beyond static medical vision tasks, to those requiring spatial reasoning and contextual understanding of anatomical structures.

To address these challenges, we introduce **U2-BENCH**, the first benchmark holistically evaluating current LVLMs for ultrasound understanding across diverse tasks and anatomies. The dataset we use comprises 7,241 cases across 15 anatomical regions, involving breast, heart, lung, etc, covering 8 diverse clinical tasks and 50 application scenarios. Each task belongs to one of the four categories: (1) classification (i.e., disease diagnosis, view recognition and assessment), (2) detection (i.e., lesion localization, organ detection, keypoint detection), (3) regression (i.e., clinical value estimation), (4) text generation (i.e., report generation, caption generation). Samples are selected to ensure balance across data sources, anatomies, and task types, to enable robust evaluation and alleviate dataset-specific bias. Several examples in our **U2-BENCH** are shown in Fig. 1.

We benchmark 20 LVLMs, including both open- and closed-source, general-purpose and medical-specialized models, on a diverse set of US tasks. **U2-BENCH** makes the following key contributions:

- **Comprehensive Dataset:** We release the first publicly available benchmark comprising 7,241 ultrasound cases spanning 15 anatomies and 8 clinical tasks, covering 50 application scenarios. Each case is annotated with task-aligned labels in a unified format and paired with carefully designed prompts, enabling standardized and reproducible evaluation.

- **Task Suite and Evaluation:** We define an eight-task taxonomy spanning *disease diagnosis, view recognition and assessment, lesion localization, organ detection, keypoint detection, clinical value estimation, report generation, and caption generation*. Each task reflects real-world clinical workflows and is paired with standard evaluation metrics. We also introduce an aggregate metric to provide a unified assessment of each model’s overall capability in ultrasound understanding.
- **Empirical Insights:** We conduct the first large-scale evaluation of LVLMs on ultrasound, uncovering consistent trends across model families: models achieve strong performance on image-level disease diagnosis and clinical value estimation tasks, but degrade on spatial reasoning tasks such as view recognition and organ detection. Clinical report generation tasks remain particularly challenging. Performance gains from model scaling can be limited, and compact models occasionally outperform larger ones on certain tasks, suggesting that targeted training may be more impactful than scale alone in ultrasound understanding.

2 RELATED WORK

Large Vision-Language Models. LVLMs such as GPT-4V (OpenAI, 2023), Claude (Anthropic, 2024), Gemini (Anil et al., 2023), DeepSeek-VL (DeepSeek-AI et al., 2024), LLaVA (Liu et al., 2023a), Qwen-VL (Bai et al., 2023b), and MiniGPT4 (Zhu et al., 2023) have emerged as general-purpose multimodal systems capable of handling tasks like image captioning, visual question answering, and multimodal reasoning. These models are trained on large-scale image-text pairs (Sharma et al., 2018; Schuhmann et al., 2022), and their performance has been extensively evaluated in domains such as question answering, mathematics, and science (Chen et al., 2021; Sun et al., 2023; Wang et al., 2023; Huang et al., 2022; Liu et al., 2023b). However, their clinical reliability remains underexplored.

To address this gap, several medical-specialized LVLMs have been proposed. MiniGPT-Med (Wu et al., 2023b) focuses on X-ray, CT, and MRI for tasks such as medical report generation, VQA, and disease identification. RadFM (Wu et al., 2023a) further supports both 2D and 3D modalities. MedDr (He et al., 2024) extends to radiology, pathology, dermatology, retinography, and endoscopy, introducing a retrieval-augmented diagnosis strategy. Lingshu (Xu et al., 2025) is a recent medical LVLM that covers multiple imaging modalities. Yet, these models exclude ultrasound. Med-Gemini (Team, 2024) and MedGemma (Sellergren et al., 2025) span numerous modalities including ultrasound, though their capability in this domain is limited to caption generation.

Multimodal Benchmarks for Large Vision-Language Models. Several benchmarks assess general-domain LVLMs. MMBench (Liu et al., 2023c), MMT-Bench (Ying et al., 2024), and SEED-Bench (Li et al., 2023a) evaluate general-domain LVLMs through bilingual multiple-choice questions, large-scale visual reasoning tasks, and generative comprehension across image and video VQA, respectively. However, these benchmarks emphasize general-purpose visual understanding and omit clinically grounded evaluation.

Early medical VQA datasets like VQA-RAD (Lau et al., 2018), VQA-Med (Ben Abacha et al., 2019), and PathVQA (He et al., 2020) offer radiology or pathology image–question pairs but are not designed for evaluating LVLMs. GMAI-MMBench (Chen et al., 2024a) introduces a large-scale VQA-style benchmark for medical LVLMs, yet it contains only about 1.4k ultrasound cases primarily focused on classification and segmentation on 6 anatomies, and does not evaluate broader model capabilities such as clinical value estimation or structured report generation. In contrast, our **U2-BENCH** focuses exclusively on ultrasound and includes a diverse set of clinically meaningful tasks and anatomical regions. We have also included a comparison with existing ultrasound foundational datasets in Appendix A.

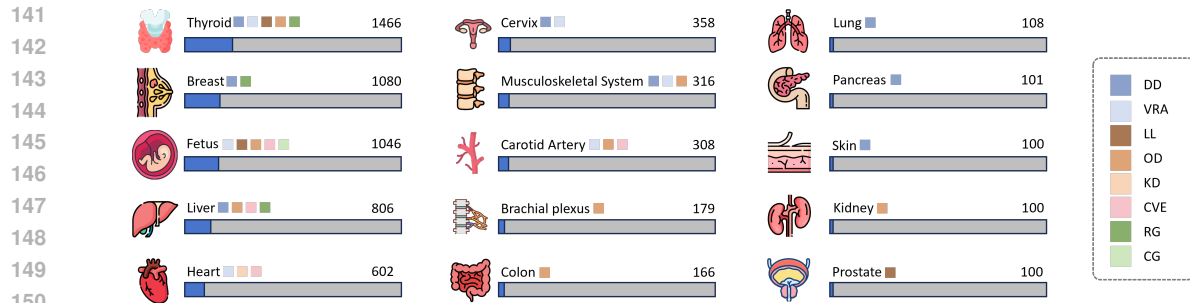


Figure 2: **Distribution of benchmark tasks across 15 anatomical regions in U2-BENCH.** The colored boxes next to each anatomy name indicate the benchmark tasks available for that anatomy, with each color corresponding to one of the eight core tasks (legend shown on the right). **The blue bar represents the total number of samples for each anatomy region, with its length proportional to the sample count.** Multiple tasks may share samples from the same anatomical region, depending on annotation availability and clinical relevance.

3 U2-BENCH

Overview. **U2-BENCH** is designed to holistically assess the capabilities of LVLM in ultrasound tasks. Section 3.1 introduces the eight clinically inspired tasks involved in our evaluation, which reflect essential diagnostic and reasoning abilities in ultrasound understanding. Section 3.2 details our benchmark construction pipeline, including dataset curation, preprocessing, and task-specific prompting. Section 3.3 summarizes the statistical property of the resulting dataset, which comprises 7,241 cases across 15 anatomies.

3.1 TASK DEFINITIONS

U2-BENCH focuses on four core capabilities: classification, detection, regression, and text generation, to systematically evaluate the performance of LVLMs on ultrasound-related tasks. We define eight tasks based on common ultrasound use cases, designed to probe a range of multimodal abilities, including anatomy recognition and clinical reporting. The task set was informed by typical sonography workflows and refined with input from domain experts to ensure practical relevance. Together, these tasks provide a structured benchmark for assessing LVLM performance across diverse ultrasound application scenarios. The eight tasks are as follows:

Disease Diagnosis (DD). This task requires the model to identify the presence and severity of a disease condition, such as grading in the Breast Imaging Reporting and Data System, based on the appearance of the ultrasound image. The task evaluates the ability of LVLMs to extract high-level semantic features and generate clinically aligned diagnostic predictions.

View Recognition and Assessment (VRA). In clinical practice, accurate diagnosis relies on the clear presentation of anatomical structures from specific angles, referred to as ultrasound standard planes. This task evaluates the ability of a model to assess image quality and classify scans into standard planes corresponding to different anatomical structures, such as the fetal head or abdominal long axis.

Lesion Localization (LL). Given a diagnostic image, the LVLM is asked to identify the location of a lesion, such as a suspicious breast mass, by selecting from nine predefined spatial categories such as upper left, center, or lower right. This task evaluates the spatial reasoning, saliency alignment, and ability to detect subtle structural abnormalities of LVLMs.

188 **Organ Detection (OD).** This task involves identifying the presence and boundaries of target organs in
 189 the ultrasound field of view, such as liver, kidney, or nerve. It assesses coarse-grained visual recognition
 190 under challenges unique to ultrasound, such as acoustic shadowing, inter-patient variability, and orientation
 191 ambiguity from manual probe handling.

192 **Keypoint Detection (KD).** In measurement tasks such as fetal biometry and adult echocardiography, precise
 193 localization of anatomical landmarks is critical for deriving clinically meaningful measurements. This task
 194 evaluates the fine-grained spatial understanding and geometric reasoning ability of the model, which are
 195 essential for tasks like skeletal length and chamber size estimation.

196 **Clinical Value Estimation (CVE).** This task involves predicting continuous clinical parameters derived from
 197 ultrasound images, such as lesion size, left ventricular ejection fraction, or liver fat percentage. It covers both
 198 anatomical and functional indicators relevant to diagnosis, treatment planning, and longitudinal monitoring,
 199 and evaluates whether the model can perform image-to-value regression by mapping visual inputs to clinically
 200 meaningful quantitative outputs.

201 **Report Generation (RG).** The model is prompted to generate a structured clinical report based on visual
 202 input, following the format of example reports provided in the prompt. This task evaluates the ability of
 203 LVLM to perform medical language generation and produce outputs that align with standard ultrasound
 204 reporting practices.

205 **Caption Generation (CG).** The model is asked to generate a concise anatomical description of a diagnostic
 206 image, guided by example captions provided in the prompt. This task evaluates basic visual-language
 207 alignment and the ability to verbalize structural features in a clinically appropriate manner of LVLM.

210 3.2 DATA CURATION AND PROCESSING

211 In this section, following the approach of previous benchmark constructions Chen et al. (2024c); Xu et al.
 212 (2023); Zhong et al. (2023), we outline the three key steps used to build **U2-BENCH**: (1) data collection and
 213 sampling (2) data cleaning, format unification and quality verification, and (3) task-specific prompt design.
 214 Figure 3 summarizes the data processing pipeline.

215 **Data Selection and Sampling.** We construct **U2-BENCH** by sampling 7,241 ultrasound studies from 40
 216 licensed datasets. These datasets were selected to represent a wide range of diagnostic tasks, anatomical
 217 regions, and clinical contexts. While the original datasets were independently curated and clinically annotated,
 218 we performed standardization, sampling, and quality checks to ensure consistency across tasks and enable
 219 reliable, reproducible benchmarking. Some datasets contribute to multiple benchmark tasks based on their
 220 available annotations and clinical relevance.

221 To reflect real-world clinical data distributions and prevent data leakage, we adopt a task-specific, patient-level
 222 sampling strategy. Sampling is performed at the subject level rather than the image level to preserve intra-
 223 patient consistency. Importantly, during the sampling stage, datasets corresponding to clinically high-priority
 224 but data-sparse tasks were intentionally oversampled based on guidance from collaborating clinicians. To
 225 ensure anatomical coverage, we include data from 15 anatomical regions: fetus, thyroid, breast, heart, liver,
 226 cervix, carotid artery, musculoskeletal system, kidney, prostate, skin, lung, pancreas, brachial plexus, and
 227 colon.

228 **Data Cleaning, Format Unification, and Quality Verification.** All data in **U2-BENCH** are standardized
 229 into a unified format to support consistent parsing and evaluation across the dataset. Ultrasound scans are
 230 converted to a uniform image format. For video sequences, a small number of representative frames are
 231 sampled per study to control evaluation cost while retaining key diagnostic content. Task-relevant metadata,
 232 including anatomy labels, measurements, and reports, is preserved in a structured schema. Segmentation

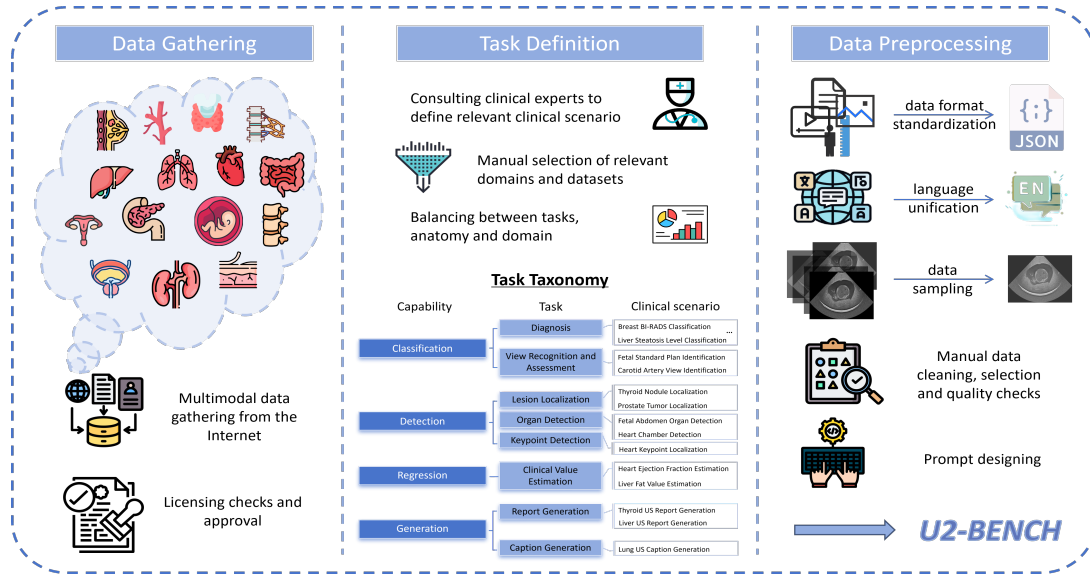


Figure 3: **Overview of the U2-BENCH construction pipeline.** The benchmark is built through three stages: (1) data gathering from 40 licensed ultrasound datasets spanning 15 anatomical regions, (2) task definition across 8 clinically inspired tasks grouped into four core capabilities: classification, detection, regression, and text generation, (3) data preprocessing, including annotation standardization, metadata unification, image/frame selection, and quality verification. This unified pipeline ensures benchmark consistency and clinical relevance across diverse ultrasound scenarios.

masks are converted to bounding boxes. Texts are translated into English using a medically guided translation pipeline, with ambiguous terms resolved via a curated glossary and final verification by clinicians.

To ensure the reliability of **U2-BENCH**, we adopt both automated and manual quality assurance procedures during data preparation.

(1) Automated Filtering. During data preprocessing, we systematically check for missing labels, inconsistent or invalid annotations, and corrupted or unreadable files. Samples that fail these checks are discarded.

(2) Manual Verification. A team of 10 annotators manually reviewed all cases using a cross-validation protocol, where each data point was independently assessed by at least three annotators. Specifically, an engineer first check the validity of the metadata in the json file, then a biomedical expert independently checked for label-image consistency, measurement units and standardized anatomical terminology. A clinician then performed a final review of the diagnostic consistency on all processed cases while writing the task-specific prompts.

Task-Specific Prompt Designing. To ensure consistent model behavior and fair comparability across tasks, we design structured prompts for each of the 50 application scenarios, consisting of three components: (1) a clinical role definition to set context and expertise, (2) a task-specific instruction aligned with standard sonography workflow, and (3) an output format specification, such as classification options, value ranges, or reference output examples. Detailed prompts are included in Appendix D. An ablation study on the impact of prompt design is presented in Section 5.2.

282 3.3 STATISTICS
283284 **U2-BENCH** comprises 7,241 ultrasound studies spanning 8 benchmark tasks and 15 anatomical regions.
285 Table 5 in Appendix C details the number of cases per task. Classification and detection constitute the largest
286 shares, with 2,999 and 2,921 cases, respectively, while generation and regression tasks provide targeted
287 evaluation of report synthesis and clinical value estimation.288 Figure 2 summarizes the distribution across anatomical regions. Thyroid and breast ultrasound together
289 account for more than one-third of all cases. This is because of their high clinical prevalence and broad
290 diagnostic utility. Many anatomies support multiple tasks - for instance, fetal ultrasound is used for classifica-
291 tion and regression - enabling multi-task evaluation within a unified anatomical context. This composition
292 ensures broad coverage across modalities, tasks, and body regions, supporting robust and clinically grounded
293 assessment of LVLM performance.294
295 4 EXPERIMENT
296297 4.1 EVALUATION SETTINGS
298299 We evaluated **U2-BENCH** on 20 LVLMs, both open-source and closed-source. A detailed list of the [exact](#)
300 [model versions evaluated and additional experimental details are provided in Appendix C, with the full](#)
301 [implementation and hyperparameter configurations available in our public code repository](#). Detailed prompts
302 are given in Appendix D.303
304 4.2 EVALUATION PROTOCOL
305306 We employed standard metrics aligned with clinical relevance and prior LVLM benchmarks. Classification
307 tasks were evaluated with accuracy and F1 score. [For detection-related tasks, we initially evaluated models](#)
308 [using the ground-truth bounding box or coordinate outputs](#). However, many LVLMs failed to reliably generate
309 valid coordinates or follow bounding-box formatting instructions. To enable stable and comparable evaluation
310 across models, we therefore simplified the detection tasks into a 9-class position-classification formulation,
311 where each region corresponds to a coarse spatial sector of the image. Under this formulation, detection tasks
312 utilized accuracy as the metric to assess localization correctness. Regression tasks report Root Mean Squared
313 Error (RMSE), Mean Absolute Error (MAE), and percentage within tolerance (%_tol). Generation tasks were
314 assessed with BLEU-4 as percentage, ROUGE, and BERTScore (Zhang* et al., 2020) to capture both lexical
315 and semantic similarity. All metrics were computed using ground-truth labels from the original dataset and
316 standardized outputs with the format specified by the prompts across models to ensure fair comparison.317 **U2-Score.** We design a quantitative score to provide an overall evaluation metric for the ultrasound
318 understanding capability of a model. The **U2-SCORE** is defined as a weighted combination of the metrics
319 across all tasks, [which is mathematically equivalent to computing a case-level average, consistent with prior](#)
320 [work \(Chen et al., 2024a\)](#). This can be formulated as:

321
322
$$\text{U2-Score} := \sum_{t=1}^N w_t d_t, \text{ where } w_t = \frac{n_t}{\sum_j n_j}, \text{ and } d_t \leq 1 \quad (1)$$

323
324

325 where N represents the number of tasks, w_t is the corresponding task weight, which is computed from the
326 proportion of the sample number n_t of the t -th task. This can mitigate the imbalance issue of sample size in
327 different tasks. Here, d_t denotes the value of the selected metric of the t -th task. More details are included in
328 Appendix C.

329 4.3 EVALUATION RESULTS
330331 We present a comprehensive comparison of multimodal models on the **U2-BENCH** benchmark (Table 1),
332 aiming to identify key performance trends across tasks and model types. A more detailed example cases and
333 error analysis is included in Appendix C.
334335 **Closed-Source Models Lead.** Closed-source models continue to dominate, with **Dolphin-V1** achieving the
336 highest overall score of **0.5835**, substantially outperforming all other models. The next strongest proprietary
337 model, **GPT-5**, reaches a U2-Score of **0.3250**, followed by **Gemini-2.5-Pro-Preview** at **0.2968**. While the
338 best open-source model, **DeepSeek-VL2**, attains a competitive score of **0.2630**, the gap to closed-source
339 systems remains significant. These results highlight that despite rapid advances in open-source approaches,
340 closed-source models still benefit from access to larger proprietary datasets and tailored optimization, giving
341 them a clear performance edge.
342343 **Task Difficulty Varies Significantly.** Image classification tasks remain the most tractable, with **Dolphin-V1**
344 achieving the highest accuracy of **0.682** on **DD**, and several other models exceeding 0.48. In contrast, spatial
345 reasoning and text generation remain difficult: no model surpasses **0.160** accuracy on **KD**, and all models fall
346 below **7.5 BLEU** on **RG**. Regression tasks are also challenging; only the closed-source **Qwen-Max** reduces
347 RMSE to **0.1248**, while all open-source models remain above **0.1675**.
348349 **Scaling Brings Diminishing Returns.** Within the **Qwen-2.5-VL** family, scaling from 3B to 72B parameters
350 yields consistent performance gains. While larger models achieve lower **CVE** RMSE, improvements in
351 language generation and spatial reasoning tasks plateau, suggesting that excessive scaling may lead to
352 overfitting on superficial visual patterns, ultimately harming clinical text generation capabilities.
353354 **Domain-Specific Models Excel in Reasoning.** Medical-domain models such as **MedDr** show competitive
355 performance on reasoning tasks (e.g., **CVE** RMSE = 0.214; **CG BERT** = 81.21), outperforming many general-
356 purpose systems in structured clinical evaluation. Similarly, **MedGemma-4B-it** achieves the second-best **CVE**
357 performance (RMSE = 0.167), highlighting the advantage of domain adaptation for quantitative reasoning.
358 However, these models still lag behind larger general multimodal models on visual classification. For example,
359 **Qwen-72B** achieves a **DD** F1 of 0.456, compared to **MedDr**'s 0.312. This suggests that domain-specialized
360 models are particularly effective for semantic and reasoning-heavy tasks, while general-purpose models retain
361 an edge in coarse-grained visual recognition.
362

4.4 LIMITATIONS AND FUTURE OUTLOOK FOR ULTRASOUND LVLMS

363 While existing LVLMS demonstrate impressive general multimodal capabilities, our results reveal fundamental
364 limitations in ultrasound-specific perception and clinical reasoning.
365366 **Weak Perception of Ultrasound Structures.** Models struggle with recognizing relative spatial relationships
367 between anatomical structures, as reflected by their poor performance on detection tasks, and often fail to
368 capture subtle echogenicity patterns that are essential for clinical diagnosis. This likely stems from the lack of
369 large-scale ultrasound-specific image–caption pretraining data and the inherently noisy, heterogeneous nature
370 of ultrasound imaging. Improving perception would require curated ultrasound datasets, ultrasound-aware
371 pretraining objectives, and architectures or adapters with explicit spatial-reasoning capabilities.
372373 **Clinical Ultrasound Tasks Are Far More Complex Than Generic Vision-Language Tasks.** Ultrasound
374 spans more than 15 clinical subspecialties, each with distinct anatomical structures, scanning planes, and
375 diagnostic criteria. For example, fetal biometry requires standardized abdominal circumference (AC) or head

376 Table 1: Results of different models on the **U2-BENCH**. We utilize green (1st), blue (2nd), and yellow
 377 (3rd) backgrounds to distinguish the top three results within different models. The “U2-Score” column
 378 represents the quantitative score defined in Section 4.2. To calculate the **U2-SCORE** for random guessing, the
 379 BLEU scores are taken to be zero.

Models	DD		VRA		LL		OD		KD		CVE			RG			CG			U2-Score ↑
	Acc. ↑	F1 ↑	Acc. ↑	F1 ↑	Acc. ↑	Acc. ↑	Acc. ↑	Acc. ↑	RMSE ↓	MAE ↓	%tol ↑	BLEU% ↑	Rouge% ↑	BERT% ↑	BLEU% ↑	Rouge% ↑	BERT% ↑			
Random Guessing	0.4143	0.4135	0.3195	0.3184	0.1118	0.0680	0.1120	0.5472	0.4352	18.776	-	-	-	-	-	-	-	-		
<i>Medical-Specific Models</i>																				
MiniGPT-Med	0.3468	0.2828	0.1800	0.1048	0.1728	0.1789	0.0840	0.3056	0.2600	33.2259	6.4700	20.1300	74.6900	30.2000	47.7500	80.5000	0.2375			
MedDr	0.4508	0.3118	0.2071	0.1214	0.0720	0.0881	0.0900	0.2144	0.1788	38.2642	2.7998	13.5060	72.2050	33.4939	49.6236	81.2078	0.2373			
MedGemma-4B-it	0.5005	0.4336	0.3071	0.1520	0.2750	0.0858	0.0200	0.1667	0.1316	55.0962	1.5360	15.0348	74.0205	4.8777	35.9803	76.7859	0.2668			
Lingshu-7B	0.4589	0.2755	0.2625	0.1490	0.1265	0.2005	0.1140	0.2581	0.1908	27.8302	1.9974	15.7764	67.8138	4.0058	12.3106	62.0800	0.2704			
<i>Open-Source Multimodal Models</i>																				
Qwen-2.5-VL-3B-Instruct	0.4503	0.3591	0.2097	0.1492	0.0696	0.0649	0.0898	0.5008	0.4519	18.9055	3.5018	15.0327	72.8419	27.6748	44.7618	79.8849	0.2095			
Qwen-2.5-VL-7B-Instruct	0.4821	0.3860	0.2181	0.1665	0.0750	0.0704	0.1000	0.4646	0.4337	19.7115	3.7100	15.5600	73.1500	29.4400	47.0000	81.1500	0.2235			
Qwen-2.5-VL-32B-Instruct	0.4812	0.3860	0.2864	0.2071	0.1700	0.0755	0.0880	0.3414	0.3015	27.4038	1.1900	13.0100	68.1400	14.7700	38.6800	77.3900	0.2449			
Qwen-2.5-VL-72B-Instruct	0.4895	0.4556	0.2559	0.1789	0.1150	0.0660	0.0860	0.3224	0.2733	37.9370	3.0900	15.0600	72.6600	28.1600	44.2800	80.9100	0.2421			
DeepSeek-VL2	0.4126	0.3190	0.2268	0.1111	0.2950	0.1682	0.1320	0.2956	0.2505	12.3355	7.4700	20.5400	75.3800	11.4200	34.8500	77.2400	0.2630			
InternVL3-9B-Instruct	0.4447	0.3716	0.1926	0.1083	0.3000	0.1416	0.0940	0.2429	0.1733	50.8738	2.1600	14.7000	72.2100	21.5900	43.1300	80.9800	0.2566			
LLaVA-1.5-13B	0.4321	0.3055	0.1731	0.0755	0.1700	0.1259	0.1100	0.2307	0.1976	24.7964	6.2400	18.5800	73.7900	10.8300	29.4000	75.5000	0.2378			
Phi-4-Multimodal-Instruct	0.3686	0.1148	0.2452	0.0537	0.0350	0.0815	0.1600	0.2249	0.2006	16.1972	3.2700	16.5800	73.2700	3.8700	22.9800	73.0800	0.2168			
Mistral-Small-3.1-24B-Inst	0.4359	0.0936	0.1964	0.0664	0.1300	0.0910	0.1060	0.1675	0.1331	45.9459	1.8000	14.9000	71.7200	20.7700	42.1200	80.7400	0.2356			
<i>Closed-Source Multimodal Models</i>																				
Doubaao-1.5-Vision-Pro-32k	0.5580	0.2597	0.2922	0.2147	0.1700	0.0729	0.1240	0.3664	0.3377	33.1731	0.7100	6.6450	72.4000	8.6400	33.3000	78.4200	0.2587			
GPT-4o-Mini	0.4924	0.3784	0.1922	0.1272	0.1357	0.0846	0.0960	0.2267	0.1976	19.2308	4.9400	17.5200	74.1300	11.7300	36.2900	77.5300	0.2388			
GPT-4o	0.4928	0.4132	0.1504	0.0974	0.1161	0.0850	0.0840	0.3712	0.3527	15.7895	2.6800	14.7700	73.3500	33.7700	49.9600	81.5800	0.2253			
GPT-5	0.5366	0.4590	0.4573	0.3550	0.2662	0.1767	0.1080	0.3097	0.1878	36.1867	1.0641	8.7440	66.8302	7.9669	23.3116	72.2203	0.3250			
Gemini-1.5-Pro	0.3781	0.2247	0.0990	0.0476	0.2700	0.0661	0.0980	0.2772	0.2205	40.7051	0.5800	9.9400	70.5500	28.5800	45.9200	80.0200	0.1999			
Gemini-2.0-Pro-Exp	0.4925	0.4194	0.1648	0.1323	0.1714	0.0945	0.0820	0.1945	0.1498	53.3333	0.2600	6.9200	40.2400	31.1800	48.6000	81.6000	0.2438			
Gemini-2.5-Pro-Preview	0.4256	0.3112	0.2099	0.1493	0.2709	0.2714	0.2518	0.2937	0.2672	34.4970	5.5030	18.0180	74.4930	15.0110	38.0070	75.9890	0.2968			
Claude-3.7-Sommet	0.2121	0.0449	0.1453	0.0479	0.1356	0.0540	0.0760	0.1764	0.1500	36.0215	0.6900	12.2300	68.7400	1.2900	16.6600	71.6600	0.1596			
Qwen-Max	0.4566	0.2676	0.1925	0.0871	0.1606	0.0761	0.0940	0.1248	0.0843	69.2308	3.5000	17.0200	73.9600	30.6700	49.0000	82.5500	0.2445			
Dolphin-V1	0.6819	0.5155	0.6943	0.5821	0.4775	0.6003	0.5080	0.2430	0.2273	38.6458	3.2193	15.1170	72.7287	54.0634	76.0111	92.9601	0.5835			

DD = Disease Diagnosis; VRA = View Recognition and Assessment; LL = Lesion Localization; OD = Organ Detection;
 KD = Keypoint Detection; CVE = Clinical Value Estimation; RG = Report Generation; CG = Caption Generation.

399 circumference (HC) views, while cardiac ultrasound relies on parasternal long-axis or apical four-chamber
 400 views. A clinically useful LVLM must therefore understand specialty-specific anatomy, follow established
 401 scanning protocols, and reason according to diagnostic workflows.

5 ANALYSIS

5.1 INSTRUCTION FOLLOWING ANALYSIS

409 Table 2 shows that contemporary models are already highly adept at parsing prompts and adhering to output
 410 specifications: six of the seventeen systems achieve a perfect score on the DD benchmark. The remaining
 411 models lag only slightly behind. The medical-oriented MiniGPT-Med (Alkhaldi et al., 2024) and MedDr (He
 412 et al., 2024) deliver middling results, while Qwen-3B and Qwen-72B (Bai et al., 2023b) close the gap rapidly
 413 as their parameter counts increase. Claude-3.7 (Anthropic, 2025) score of 0.942 is largely attributable to
 414 occasional formatting omissions. For every non-perfect model, the deviation from the maximum is under
 415 six percentage points, and no systematic failures are observed. **We also note that some models occasionally**
 416 **refuse to answer due to internal safety constraints, producing responses such as “insufficient information” or**
 417 **“I cannot provide medical advice”, rather than simply failing to follow instructions.**

418
 419 Table 2: Instruction following comparison across different models.
 420

Task	Models																
	MiniGPT-Med	MedDr	Qwen-3B	Qwen-7B	Qwen-32B	Qwen-72B	Dolphin-V1	DeepSeek	InternVL	LLaVA	Phi-4	Mistral	Doubaao-1.5	GPT-4o	Gem-2.0	Gem-2.5	Claude-3.7
DD	0.952	0.961	0.968	0.983	0.996	1.000	1.000	1.000	0.993	0.987	0.998	0.999	1.000	1.000	0.997	1.000	0.942

423 5.2 PROMPT WITH OR WITHOUT ANATOMY
424425 We investigate whether explicitly naming the anatomical region in the prompt significantly changes the
426 diagnostic accuracy of LVLMs in ultrasound. To this end, we treat the two prompt variants as paired
427 conditions applied to the same set of inputs and evaluate the statistical significance of their differences using
428 McNemar’s test.429 Specifically, for each image x_i , we generate two prompts:
430431 **With anatomy:** “You are a radiologist analysing a {anatomy} ultrasound image, please analyze...”
432 **No anatomy:** “You are a radiologist analysing an ultrasound image, please analyze...”433 Each prompt–image pair is forward-passed through the model five times, with the final prediction determined
434 by majority vote. This produces paired outcomes ($y_i^{\text{with}}, y_i^{\text{without}}$) for each image. Experiment was conducted
435 on 521 breast and thyroid studies from our dataset, the following paired contingency table presents the result
436 for model Gemini-2.0-Pro-Exp:
437438 **Table 3: Effect of anatomy tokens in prompt design.** Paired outcomes of 521 samples comparing prompts
439 with and without anatomy tokens. Each entry shows the number of samples in that outcome combination.
440

		No-anatomy prompt	
With-anatomy prompt		Correct	Incorrect
Correct		209 (<i>both correct</i>)	64 (<i>only anatomy correct</i>)
Incorrect		26 (<i>only no-anatomy correct</i>)	222 (<i>both incorrect</i>)

447 McNemar’s exact test yields a test statistic $\chi^2 = 16.04$ with $p = 6.2 \times 10^{-5}$, providing strong evidence that
448 the two conditions differ. Specifically, prompts with anatomy tokens achieve an accuracy of 52.4% versus
449 45.1% without, a gain of +7.3 percentage points.450 The McNemar test confirms that the inclusion of anatomy information in the prompt significantly improves
451 diagnostic accuracy, rejecting the null hypothesis of no difference between prompt types.
452453 6 CONCLUSION
454455 Ultrasound is essential to global healthcare but remains difficult to interpret. We present **U2-BENCH**, the
456 first benchmark for evaluating LVLMs on ultrasound understanding. It includes 7,241 cases across 15
457 anatomical regions and defines 8 clinical tasks for 50 application scenarios. Evaluating 20 LVLMs, we
458 find their strong performance in classification but persistent challenges in spatial reasoning and clinical text
459 generation, suggesting a future direction for improving LVLMs on ultrasound interpretation.
460

470 **Reproducibility Statement** We have taken extensive measures to ensure the reproducibility of our work.
 471 The benchmark dataset (7,241 ultrasound cases across 15 anatomies and 8 tasks) is publicly available on
 472 HuggingFace, and the complete evaluation toolkit is released anonymously at <https://anonymous.4open.science/r/U2-Bench-F781/VLMEVALKIT/>. Detailed descriptions of dataset curation, preprocessing, and
 473 quality verification procedures are provided in Section 3.2 and Appendix C–D, including sampling strategies,
 474 annotation protocols, and prompt templates. The full list of models evaluated, along with task-specific
 475 metrics and the aggregate U2-Score formulation, is given in Section 4.2 and Appendix C. For reproducibility
 476 of theoretical and statistical analyses (e.g., McNemar test for prompt design), contingency tables and test
 477 statistics are reported in Section 5.2.
 478

480 REFERENCES

481 Marah I Abdin, Jyoti Aneja, Harkirat S. Behl, Sébastien Bubeck, Ronen Eldan, Suriya Gunasekar, Michael
 482 Harrison, Russell J. Hewett, Mojan Javaheripi, Piero Kauffmann, James R. Lee, Yin Tat Lee, Yuanzhi
 483 Li, Weishung Liu, Caio C. T. Mendes, Anh Nguyen, Eric Price, Gustavo de Rosa, Olli Saarikivi, Adil
 484 Salim, Shital Shah, Xin Wang, Rachel Ward, Yue Wu, Dingli Yu, Cyril Zhang, and Yi Zhang. Phi-
 485 4 technical report. *CoRR*, abs/2412.08905, 2024. doi: 10.48550/ARXIV.2412.08905. URL <https://doi.org/10.48550/arXiv.2412.08905>.

486 Walid Al-Dhabyani, Mohammed Gomaa, Hussien Khaled, and Aly Fahmy. Dataset of breast ultrasound
 487 images. *Data in Brief*, 28:104863, 2020. ISSN 2352-3409. doi: <https://doi.org/10.1016/j.dib.2019.104863>.
 488 URL <https://www.sciencedirect.com/science/article/pii/S2352340919312181>.

489 Asma Alkhaldi, Raneem Alnajim, Layan Alabdullatef, Rawan Alyahya, Jun Chen, Deyao Zhu, Ahmed
 490 Alsinan, and Mohamed Elhoseiny. Minigpt-med: Large language model as a general interface for radiology
 491 diagnosis. *arXiv preprint arXiv:2407.04106*, 2024.

492 Rohan Anil, Sebastian Borgeaud, Yonghui Wu, Jean-Baptiste Alayrac, Jiahui Yu, Radu Soricut, Johan
 493 Schalkwyk, Andrew M. Dai, Anja Hauth, Katie Millican, David Silver, Slav Petrov, Melvin Johnson,
 494 Ioannis Antonoglou, Julian Schrittwieser, Amelia Glaese, Jilin Chen, Emily Pittler, Timothy P. Lillicrap,
 495 Angeliki Lazaridou, Orhan Firat, James Molloy, Michael Isard, Paul Ronald Barham, Tom Hennigan,
 496 Benjamin Lee, Fabio Viola, Malcolm Reynolds, Yuanzhong Xu, Ryan Doherty, Eli Collins, Clemens Meyer,
 497 Eliza Rutherford, Erica Moreira, Kareem Ayoub, Megha Goel, George Tucker, Enrique Piqueras, Maxim
 498 Krikun, Iain Barr, Nikolay Savinov, Ivo Danihelka, Becca Roelofs, Anaïs White, Anders Andreassen,
 499 Tamara von Glehn, Lakshman Yagati, Mehran Kazemi, Lucas Gonzalez, Misha Khalman, Jakub Sygnowski,
 500 and et al. Gemini: A family of highly capable multimodal models. *CoRR*, abs/2312.11805, 2023.

501 Anthropic. Claude 3.5 sonnet. *Anthropic News*, June 2024. URL <https://www.anthropic.com/news/claude-3-5-sonnet>.

502 Anthropic. Claude 3.7 sonnet. *Anthropic News*, February 2025. URL <https://www.anthropic.com/news/claude-3-7-sonnet>.

503 Jieyun Bai. Psfhs, April 2024. URL <https://doi.org/10.5281/zenodo.10969427>.

504 Jinze Bai, Shuai Bai, Yunfei Chu, Zeyu Cui, Kai Dang, Xiaodong Deng, Yang Fan, Wenbin Ge, Yu Han, Fei
 505 Huang, Binyuan Hui, Luo Ji, Mei Li, Junyang Lin, Runji Lin, Dayiheng Liu, Gao Liu, Chengqiang Lu,
 506 Keming Lu, Jianxin Ma, Rui Men, Xingzhang Ren, Xuancheng Ren, Chuanqi Tan, Sinan Tan, Jianhong Tu,
 507 Peng Wang, Shijie Wang, Wei Wang, Shengguang Wu, Benfeng Xu, Jin Xu, An Yang, Hao Yang, Jian
 508 Yang, Shusheng Yang, Yang Yao, Bowen Yu, Hongyi Yuan, Zheng Yuan, Jianwei Zhang, Xingxuan Zhang,
 509 Yichang Zhang, Zhenru Zhang, Chang Zhou, Jingren Zhou, Xiaohuan Zhou, and Tianhang Zhu. Qwen
 510 technical report. *arXiv preprint arXiv:2309.16609*, 2023a.

517 Jinze Bai, Shuai Bai, Shusheng Yang, Shijie Wang, Sinan Tan, Peng Wang, Junyang Lin, Chang Zhou,
 518 and Jingren Zhou. Qwen-vl: A frontier large vision-language model with versatile abilities. *CoRR*,
 519 abs/2308.12966, 2023b.

520

521 Asma Ben Abacha, Sadid A. Hasan, Vivek V. Datla, Joey Liu, Dina Demner-Fushman, and Henning Müller.
 522 Vqa-med: Overview of the medical visual question answering task at imageclef 2019. In *Working Notes of*
 523 *CLEF 2019*, volume 2380 of *CEUR Workshop Proceedings*, Lugano, Switzerland, September 9-12 2019.
 524 CEUR-WS.org. URL https://ceur-ws.org/Vol-2380/paper_272.pdf.

525

526 Yuan Bi, Zhongliang Jiang, Ricarda Clarenbach, Reza Ghotbi, Angelos Karlas, and Nassir Navab. Mi-
 527 segnet: Mutual information-based us segmentation for unseen domain generalization, 2024. URL <https://arxiv.org/abs/2303.12649>.

528

529 Xavier P. Burgos-Artizzu, David Coronado-Gutierrez, Brenda Valenzuela-Alcaraz, Elisenda Bonet-Carne,
 530 Elisenda Eixarch, Fatima Crispi, and Eduard Gratacós. Fetal_planes_db: Common maternal-fetal ultra-
 531 soundimages, June 2020. URL <https://doi.org/10.5281/zenodo.3904280>.

532

533 Michal Byra, Grzegorz Styczynski, Cezary Szmigielski, Piotr Kalinowski, Lukasz Michalowski, Rafal
 534 Palusziewicz, Bogna Ziarkiewicz-Wroblewska, Krzysztof Zieniewicz, Piotr Sobieraj, and Andrzej Now-
 535 icki. Dataset of b-mode fatty liver ultrasound images, August 2018. URL <https://doi.org/10.5281/zenodo.1009146>.

536

537 ByteDance. Doubao model series. <https://www.doubao.com/>, 2024. Accessed: 2025-05-14.

538

539 Mark Chen, Jerry Tworek, Heewoo Jun, Qiming Yuan, Henrique Ponde de Oliveira Pinto, Jared Kaplan, Harri
 540 Edwards, Yuri Burda, Nicholas Joseph, Greg Brockman, et al. Evaluating large language models trained
 541 on code. *arXiv preprint arXiv:2107.03374*, 2021.

542

543 Pengcheng Chen, Jin Ye, Guoan Wang, Yanjun Li, Zhongying Deng, Wei Li, Tianbin Li, Haodong Duan,
 544 Ziyan Huang, Yanzhou Su, Benyou Wang, Shaoting Zhang, Bin Fu, Jianfei Cai, Bohan Zhuang, Eric J
 545 Seibel, Junjun He, and Yu Qiao. Gmai-mmbench: A comprehensive multimodal evaluation benchmark
 546 towards general medical ai, 2024a. URL <https://arxiv.org/abs/2408.03361>.

547

548 Pengcheng Chen, Jin Ye, Guoan Wang, Yanjun Li, Zhongying Deng, Wei Li, Tianbin Li, Haodong Duan,
 549 Ziyan Huang, Yanzhou Su, Benyou Wang, Shaoting Zhang, Bin Fu, Jianfei Cai, Bohan Zhuang, Eric J
 550 Seibel, Yu Qiao, and Junjun He. Gmai-mmbench: A comprehensive multimodal evaluation benchmark
 551 towards general medical ai. In A. Globerson, L. Mackey, D. Belgrave, A. Fan, U. Paquet, J. Tomczak,
 552 and C. Zhang (eds.), *Advances in Neural Information Processing Systems*, volume 37, pp. 94327–94427.
 553 Curran Associates, Inc., 2024b. URL https://proceedings.neurips.cc/paper_files/paper/2024/file/ab7e02fd60e47e2a379d567f6b54f04e-Paper-Datasets_and_Benchmarks_Track.pdf.

554

555 Zhuang Chen, Jincenzi Wu, Jinfeng Zhou, Bosi Wen, Guanqun Bi, Gongyao Jiang, Yaru Cao, Mengting
 556 Hu, Yunghwei Lai, Zexuan Xiong, and Minlie Huang. Tombench: Benchmarking theory of mind in large
 557 language models. In Lun-Wei Ku, Andre Martins, and Vivek Srikumar (eds.), *Proceedings of the 62nd*
 558 *Annual Meeting of the Association for Computational Linguistics (Volume 1: Long Papers)*, ACL 2024,
 559 *Bangkok, Thailand, August 11-16, 2024*, pp. 15959–15983. Association for Computational Linguistics,
 560 2024c.

561

562 Matthew Christensen, Milos Vukadinovic, Neal Yuan, and David Ouyang. Vision-language foundation model
 563 for echocardiogram interpretation. *Nature Medicine*, 30(5):1481–1488, May 2024. ISSN 1546-170X. doi:
 10.1038/s41591-024-02959-y. URL <https://doi.org/10.1038/s41591-024-02959-y>.

564 Karine Souza Da Correggio, Roberto Noya Galluzzo, Luís Otávio Santos, Felipe Soares Muylaert Barroso,
 565 Thiago Zimmermann Loureiro Chaves, Alexandre Sherley Casimiro Onofre, and Aldo von Wangenheim.
 566 Fetal abdominal structures segmentation dataset using ultrasonic images, 2023. URL <https://doi.org/10.17632/4gcpm9dsc3.1>.
 567

568 DeepSeek-AI. Deepseek-v2: A strong, economical, and efficient mixture-of-experts language model, 2024.
 569

570 DeepSeek-AI, Aixin Liu, Bei Feng, Bing Xue, Bingxuan Wang, Bochao Wu, Chengda Lu, Chenggang Zhao,
 571 Chengqi Deng, Chenyu Zhang, Chong Ruan, Damai Dai, Daya Guo, Dejian Yang, Deli Chen, Dongjie
 572 Ji, Erhang Li, Fangyun Lin, Fucong Dai, Fuli Luo, Guangbo Hao, Guanting Chen, Guowei Li, H. Zhang,
 573 Han Bao, Hanwei Xu, Haocheng Wang, Haowei Zhang, Honghui Ding, Huajian Xin, Huazuo Gao, Hui Li,
 574 Hui Qu, J. L. Cai, Jian Liang, Jianzhong Guo, Jiaqi Ni, Jiaoshi Li, Jiawei Wang, Jin Chen, Jingchang Chen,
 575 Jingyang Yuan, Junjie Qiu, Junlong Li, Junxiao Song, Kai Dong, Kai Hu, Kaige Gao, Kang Guan, Kexin
 576 Huang, Kuai Yu, Lean Wang, Lecong Zhang, Lei Xu, Leyi Xia, Liang Zhao, Litong Wang, Liyue Zhang,
 577 Meng Li, Miaojun Wang, Mingchuan Zhang, Minghua Zhang, Minghui Tang, Mingming Li, Ning Tian,
 578 Panpan Huang, Peiyi Wang, Peng Zhang, Qiancheng Wang, Qihao Zhu, Qinyu Chen, Qiushi Du, R. J. Chen,
 579 R. L. Jin, Ruiqi Ge, Ruisong Zhang, Ruizhe Pan, Runji Wang, Runxin Xu, Ruoyu Zhang, Ruyi Chen, S. S.
 580 Li, Shanghao Lu, Shangyan Zhou, Shanhua Chen, Shaoqing Wu, Shengfeng Ye, Shengfeng Ye, Shirong
 581 Ma, Shiyu Wang, Shuang Zhou, Shuiping Yu, Shunfeng Zhou, Shuting Pan, T. Wang, Tao Yun, Tian Pei,
 582 Tianyu Sun, W. L. Xiao, and Wangding Zeng. Deepseek-v3 technical report. *CoRR*, abs/2412.19437, 2024.
 583 doi: 10.48550/ARXIV.2412.19437. URL <https://doi.org/10.48550/arXiv.2412.19437>.
 584

585 Atharva Divekar and Atharva Sonawane. Leveraging ai for automatic classification of pcos using ultrasound
 586 imaging, 2024. URL <https://arxiv.org/abs/2501.01984>.
 587

588 Haodong Duan, Junming Yang, Yuxuan Qiao, Xinyu Fang, Lin Chen, Yuan Liu, Xiaoyi Dong, Yuhang Zang,
 589 Pan Zhang, Jiaqi Wang, et al. Vlmevalkit: An open-source toolkit for evaluating large multi-modality
 590 models. In *Proceedings of the 32nd ACM International Conference on Multimedia*, pp. 11198–11201,
 591 2024.

592 FALLMUD. FALLMUD: Fascicle lower leg muscle ultrasound dataset. <https://kalisteo.cea.fr/index.php/fallmud/>, 2025. Dataset composed of 812 lower leg muscle ultrasound images with segmentation
 593 masks, used for muscle structure analysis and injury prevention.

594 Xiaoqing Guo, Qianhui Men, and J. Alison Noble. MMSummary: Multimodal Summary Generation for Fetal
 595 Ultrasound Video, October 2024. URL <http://arxiv.org/abs/2408.03761>. arXiv:2408.03761 [cs].
 596

597 Sunan He, Yuxiang Nie, Hongmei Wang, Shu Yang, Yihui Wang, Zhiyuan Cai, Zhixuan Chen, Yingxue
 598 Xu, Luyang Luo, Huiling Xiang, Xi Lin, Mingxiang Wu, Yifan Peng, George Shih, Ziyang Xu, Xian
 599 Wu, Qiong Wang, Ronald Cheong Kin Chan, Varut Vardhanabhuti, Winnie Chiu Wing Chu, Yefeng
 600 Zheng, Pranav Rajpurkar, Kang Zhang, and Hao Chen. Gsco: Towards generalizable ai in medicine via
 601 generalist-specialist collaboration, 2024. URL <https://arxiv.org/abs/2404.15127>.
 602

603 Xuehai He, Yichen Zhang, Luntian Mou, Eric Xing, and Pengtao Xie. Pathvqa: 30000+ questions for medical
 604 visual question answering. *arXiv preprint arXiv:2003.10286*, 2020.

605 David W. Hewson and Nigel M. Bedforth. Closing the gap: artificial intelligence applied to ultrasound-guided
 606 regional anaesthesia. *British Journal of Anaesthesia*, 130(3):245–247, 2023. ISSN 0007-0912. doi:
 607 <https://doi.org/10.1016/j.bja.2022.12.005>. URL <https://www.sciencedirect.com/science/article/pii/S0007091222006924>.
 608

609 Wenlong Huang, Pieter Abbeel, Deepak Pathak, and Igor Mordatch. Language models as zero-shot planners:
 610 Extracting actionable knowledge for embodied agents. *arXiv preprint arXiv: Arxiv-2201.07207*, 2022.

611 Xiaoshuang Huang, Lingdong Shen, Jia Liu, Fangxin Shang, Hongxiang Li, Haifeng Huang, and Yehui Yang.
 612 Towards a multimodal large language model with pixel-level insight for biomedicine. *Proceedings of the*
 613 *AAAI Conference on Artificial Intelligence*, 39(4):3779–3787, Apr. 2025. doi: 10.1609/aaai.v39i4.32394.
 614 URL <https://ojs.aaai.org/index.php/AAAI/article/view/32394>.

615

616 Zhi Huang, Federico Bianchi, Mert Yuksekgonul, Thomas J. Montine, and James Zou. A visual–language
 617 foundation model for pathology image analysis using medical twitter. *Nature Medicine*, 29(9):2307–2316,
 618 Sep 2023. ISSN 1546-170X. doi: 10.1038/s41591-023-02504-3. URL <https://doi.org/10.1038/s41591-023-02504-3>.

619

620 Hedda Cohen Indelman, Elay Dahan, Angeles M. Perez-Agosto, Carmit Shiran, Doron Shaked, and Nati
 621 Daniel. Semantic Segmentation Refiner for Ultrasound Applications with Zero-Shot Foundation Models,
 622 April 2024. URL <http://arxiv.org/abs/2404.16325>. arXiv:2404.16325 [cs] version: 1.

623

624 Yuanfeng Ji, Haotian Bai, Chongjian GE, Jie Yang, Ye Zhu, Ruimao Zhang, Zhen Li, Lingyan Zhanng,
 625 Wanling Ma, Xiang Wan, and Ping Luo. Amos: A large-scale abdominal multi-organ benchmark for
 626 versatile medical image segmentation. In S. Koyejo, S. Mohamed, A. Agarwal, D. Belgrave, K. Cho,
 627 and A. Oh (eds.), *Advances in Neural Information Processing Systems*, volume 35, pp. 36722–36732.
 628 Curran Associates, Inc., 2022. URL https://proceedings.neurips.cc/paper_files/paper/2022/file/ee604e1bedbd069d9fc9328b7b9584be-Paper-Datasets_and_Benchmarks.pdf.

629

630 Albert Q Jiang, Alexandre Sablayrolles, Arthur Mensch, Chris Bamford, Devendra Singh Chaplot, Diego
 631 de las Casas, Florian Bressand, Gianna Lengyel, Guillaume Lample, Lucile Saulnier, et al. Mistral 7b.
 632 *arXiv preprint arXiv:2310.06825*, 2023.

633

634 Jing Jiao, Jin Zhou, Xiaokang Li, Menghua Xia, Yi Huang, Lihong Huang, Na Wang, Xiaofan Zhang,
 635 Shichong Zhou, Yuanyuan Wang, and Yi Guo. USFM: A universal ultrasound foundation model generalized
 636 to tasks and organs towards label efficient image analysis. *Medical Image Analysis*, 96:103202, August
 637 2024. ISSN 13618415. doi: 10.1016/j.media.2024.103202. URL <https://linkinghub.elsevier.com/retrieve/pii/S1361841524001270>.

638

639 Sekeun Kim, Pengfei Jin, Sifan Song, Cheng Chen, Yiwei Li, Hui Ren, Xiang Li, Tianming Liu, and
 640 Quanzheng Li. Echofm: Foundation model for generalizable echocardiogram analysis. *arXiv preprint*
 641 *arXiv:2410.23413*, 2024.

642

643 Markus Krönke, Christine Eilers, Desislava Dimova, Melanie Köhler, Gabriel Buschner, Lilit Schweiger,
 644 Lemonia Konstantinidou, Marcus Makowski, James Nagarajah, Nassir Navab, Wolfgang Weber, and
 645 Thomas Wendler. Tracked 3d ultrasound and deep neural network-based thyroid segmentation reduce
 646 interobserver variability in thyroid volumetry. *PLOS ONE*, 17(7):1–15, 07 2022. doi: 10.1371/journal.pone.0268550. URL <https://doi.org/10.1371/journal.pone.0268550>.

647

648 Jason J. Lau, Soumya Gayen, Asma Ben Abacha, and Dina Demner-Fushman. A dataset of clinically
 649 generated visual questions and answers about radiology images. *Scientific Data*, 5(1):180251, Nov 2018.
 650 ISSN 2052-4463. doi: 10.1038/sdata.2018.251. URL <https://doi.org/10.1038/sdata.2018.251>.

651

652 Alexandra Laverde Saad, Abdulhadi Jfri, Rubén García, Irene Salguero, Constanza Martínez, Hirune Cem-
 653 brero, Gastón Roustán, and Fernando Alfageme. Discriminative deep learning based benignity/malignancy
 654 diagnosis of dermatologic ultrasound skin lesions with pretrained artificial intelligence architecture. *Skin
 Research and Technology*, 28, 08 2021. doi: 10.1111/srt.13086.

655

656 Sarah Leclerc, Erik Smistad, João Pedrosa, Andreas Østvik, Frederic Cervenansky, Florian Espinosa, Torvald
 657 Espeland, Erik Andreas Rye Berg, Pierre-Marc Jodoin, Thomas Grenier, Carole Lartizien, Jan D’hooge,
 Lasse Lovstakken, and Olivier Bernard. Deep learning for segmentation using an open large-scale

658 dataset in 2d echocardiography. *IEEE Transactions on Medical Imaging*, 38(9):2198–2210, 2019. doi:
 659 10.1109/TMI.2019.2900516.

660

661 Ramona Leenings, Maximilian Konowski, Nils R. Winter, Jan Ernsting, Lukas Fisch, Carlotta Barkhau,
 662 Udo Dannlowski, Andreas Lügering, Xiaoyi Jiang, and Tim Hahn. C-trus: A novel dataset and initial
 663 benchmark for colon wall segmentation in transabdominal ultrasound. In Alberto Gomez, Bishesh Khanal,
 664 Andrew King, and Ana Namburete (eds.), *Simplifying Medical Ultrasound*, pp. 101–111, Cham, 2025.
 665 Springer Nature Switzerland. ISBN 978-3-031-73647-6.

666

667 Bohao Li, Rui Wang, Guangzhi Wang, Yuying Ge, Yixiao Ge, and Ying Shan. Seed-bench: Benchmarking
 668 multimodal llms with generative comprehension. *arXiv preprint arXiv:2307.16125*, 2023a.

669

670 Jiajia Li, Pingping Zhang, Teng Wang, Kaixuan Wang, and Bin Sheng. Lepset, June 2023b. URL <https://doi.org/10.5281/zenodo.8041285>.

671

672 Jun Li, Tongkun Su, Baoliang Zhao, Faqin Lv, Qiong Wang, Nassir Navab, Ying Hu, and Zhongliang Jiang.
 673 Ultrasound report generation with cross-modality feature alignment via unsupervised guidance, 2024. URL
 674 <https://arxiv.org/abs/2406.00644>.

675

676 Zhi Lin, Junhao Lin, Lei Zhu, Huazhu Fu, Jing Qin, and Liansheng Wang. A new dataset and a baseline
 677 model for breast lesion detection in ultrasound videos. In Linwei Wang, Qi Dou, P. Thomas Fletcher,
 678 Stefanie Speidel, and Shuo Li (eds.), *Medical Image Computing and Computer Assisted Intervention –
 679 MICCAI 2022*, pp. 614–623, Cham, 2022. Springer Nature Switzerland.

680

681 Haotian Liu, Chunyuan Li, Qingsyang Wu, and Yong Jae Lee. Visual instruction tuning, 2023a.

682

683 Xiao Liu, Hao Yu, Hanchen Zhang, Yifan Xu, Xuanyu Lei, Hanyu Lai, Yu Gu, Hangliang Ding, Kaiwen Men,
 684 Kejuan Yang, et al. AgentBench: Evaluating LLMs as agents. *arXiv preprint arXiv:2308.03688*, 2023b.

685

686 Yuan Liu, Haodong Duan, Yuanhan Zhang, Bo Li, Songyang Zhang, Wangbo Zhao, Yike Yuan, Jiaqi Wang,
 687 Conghui He, Ziwei Liu, Kai Chen, and Duhua Lin. Mmbench: Is your multi-modal model an all-around
 688 player? *arXiv:2307.06281*, 2023c.

689

690 Yaosheng Lu, Mengqiang Zhou, Dengjiang Zhi, Minghong Zhou, Xiaosong Jiang, Ruiyu Qiu, Zhanhong
 691 Ou, Huijin Wang, Di Qiu, Mei Zhong, Xiaoxing Lu, Gaowen Chen, and Jieyun Bai. The jnu-ifm dataset
 692 for segmenting pubic symphysis-fetal head. *Data in Brief*, 41:107904, 2022. ISSN 2352-3409. doi:
 693 <https://doi.org/10.1016/j.dib.2022.107904>. URL <https://www.sciencedirect.com/science/article/pii/S2352340922001160>.

694

695 Fadillah Maani, Numan Saeed, Tausifa Saleem, Zaid Farooq, Hussain Alasmawi, Werner Diehl, Ameera
 696 Mohammad, Gareth Waring, Saudabi Valappi, Leanne Bricker, and Mohammad Yaqub. FetalCLIP: A
 697 Visual-Language Foundation Model for Fetal Ultrasound Image Analysis, February 2025. URL <http://arxiv.org/abs/2502.14807>. arXiv:2502.14807 [eess] version: 1.

698

699 Azouz Maroua. Algerian ultrasound images thyroid dataset (auitd). <https://www.kaggle.com/datasets/azouzmaroua/algeria-ultrasound-images-thyroid-dataset-auitd>, 2020. Kaggle dataset containing
 700 3-class thyroid ultrasound images (Benign, Malignant, Normal) collected from hospitals in Setif,
 701 Algeria. Accessed May 2025.

702

703 Kristen M. Meiburger, Guillaume Zahnd, Francesco Faita, Christos Loizou, Catarina Carvalho, David Stein-
 704 man, Lorenzo Gibello, Rosa Maria Bruno, Francesco Marzola, Ricarda Clarenbach, Martina Francesconi,
 Andrew Nicolaides, Aurelio Campilho, Reza Ghotbi, Efthyvoulos Kyriacou, Nassir Navab, Maura Griffin,
 Andrie Panayiotou, Rachele Gherardini, Gianfranco Varetto, Elisabetta Bianchini, Constantinos Pattichis,
 Lorenzo Ghiadoni, José Rouco, and Filippo Molinari. DATASET for "Carotid Ultrasound Boundary Study

705 (CUBS): an open multi-center analysis of computerized intima-media thickness measurement systems and
 706 their clinical impact", 2021. URL <https://doi.org/10.17632/fpv535fss7.1>.

707

708 Adrien Meyer, Aditya Murali, Didier Mutter, and Nicolas Padoy. UltraSam: A Foundation Model for
 709 Ultrasound using Large Open-Access Segmentation Datasets, November 2024. URL <http://arxiv.org/abs/2411.16222>. arXiv:2411.16222 [eess] version: 1.

710

711 Yuhao Mo, Chu Han, Yu Liu, Min Liu, Zhenwei Shi, Jiatai Lin, Bingchao Zhao, Chunwang Huang, Bingjiang
 712 Qiu, Yanfen Cui, Lei Wu, Xipeng Pan, Zeyan Xu, Xiaomei Huang, Zaiyi Liu, Ying Wang, and Changhong
 713 Liang. Hover-trans: Anatomy-aware hover-transformer for roi-free breast cancer diagnosis in ultrasound
 714 images, 2022. URL <https://arxiv.org/abs/2205.08390>.

715

716 NeuronXJTU and palkia1998. Kfgnet: Source code for video classification using ultrasonic data. <https://github.com/NeuronXJTU/KFGNet>, 2023. GitHub repository, accessed May 2025. Includes Baidu
 717 Netdisk link to ultrasonic data.

718

719 S. Novin, C. Alvarez, J. B. Renner, Y. M. Golightly, and A. E. Nelson. Features of knee and multijoint
 720 osteoarthritis by sex and race and ethnicity: A preliminary analysis in the johnston county health study.
 721 *Journal of Rheumatology*, pp. jrheum.2023-0479, September 2023. doi: 10.3899/jrheum.2023-0479. Epub
 722 ahead of print, published September 15, 2023.

723

724 OpenAI. Gpt-4 technical report. *PREPRINT*, 2023.

725

726 Collaborator Pahuni Choudhary. Carotid artery ultrasound and color doppler: Multimodal carotid
 727 artery imaging with comprehensive patient health records. <https://www.kaggle.com/datasets/pahunichoudhary/carotid-artery-ultrasound-and-color-doppler>, 2023. Kaggle dataset. In-
 728 cludes ultrasound and color Doppler images from 18 patients with structured health records. Licensed
 729 under Apache 2.0. Accessed May 2025.

730

731 Anna Pawłowska, Anna Ćwierz-Pieńkowska, Agnieszka Domalik, Dominika Jaguś, Piotr Kasprzak, Rafał
 732 Matkowski, Łukasz Fura, Andrzej Nowicki, and Norbert Żołek. Curated benchmark dataset for ultrasound
 733 based breast lesion analysis. *Scientific Data*, 11(1):148, Jan 2024. ISSN 2052-4463. doi: 10.1038/s41597-024-02984-z. URL <https://doi.org/10.1038/s41597-024-02984-z>.

734

735 Lina Pedraza, Carlos Vargas, Fabián Narváez, Oscar Durán, Emma Muñoz, and Eduardo Romero. An
 736 open access thyroid ultrasound image database. In *10th International symposium on medical information
 737 processing and analysis*, volume 9287, pp. 188–193. SPIE, 2015.

738

739 Bharath Prabakaran, Paul Hamelmann, Erik Ostrowski, and Muhammad Shafique. Fpus23: An ultrasound
 740 fetus phantom dataset with deep neural network evaluations for fetus orientations, fetal planes, and
 741 anatomical features. *IEEE Access*, PP:1–1, 01 2023. doi: 10.1109/ACCESS.2023.3284315.

742

743 Hariharan Ravishankar, Rohan Patil, Vikram Melapudi, Harsh Suthar, Stephan Anzengruber, Parminder Bha-
 744 tia, Kass-Hout Taha, and Pavan Annangi. SonoSAMTrack – Segment and Track Anything on Ultrasound
 745 Images, November 2023. URL <http://arxiv.org/abs/2310.16872>. arXiv:2310.16872 [eess].

746

747 Vuppala Adithya Sairam. Ultrasound breast images for breast cancer. <https://www.kaggle.com/datasets/aryashah2k/ultrasound-breast-images-for-breast-cancer>, 2020. Kaggle dataset. CC0: Public
 748 Domain license. Accessed May 2025.

749

750 María Sofía Sappia. Acouslic-ai : Abdominal circumference operator- agnostic ultrasound measurement in
 751 low-income countries using artificial intelligence, July 2024. URL <https://doi.org/10.5281/zenodo.12697994>.

751

752 Christoph Schuhmann, Romain Beaumont, Richard Vencu, Cade Gordon, Ross Wightman, Mehdi Cherti,
 753 Theo Coombes, Aarush Katta, Clayton Mullis, Mitchell Wortsman, et al. LAION-5B: An open large-scale
 754 dataset for training next generation image-text models. *Advances in Neural Information Processing Systems*,
 755 35:25278–25294, 2022.

756 Andrew Sellergren, Sahar Kazemzadeh, Tiam Jaroensri, Atilla Kiraly, Madeleine Traverse, Timo Kohlberger,
 757 Shawn Xu, Fayaz Jamil, Cian Hughes, Charles Lau, et al. Medgemma technical report. *arXiv preprint*
 758 *arXiv:2507.05201*, 2025.

760 Carla Sendra-Balcells, Víctor M. Campello, Jordina Torrents-Barrena, Yahya Ali Ahmed, Mustafa Elattar,
 761 Benard Ohene-Botwe, Pempho Nyangulu, William Stones, Mohammed Ammar, Lamya Nawal Benamer,
 762 Harriet Nalubega Kisembo, Senai Goitom Sereke, Sikolia Z. Wanyonyi, Marleen Temmerman, Eduard
 763 Gratacós, Elisenda Bonet, Elisenda Eixarch, Kamil Mikolaj, Martin Grønnebæk Tolsgaard, and Karim
 764 Lekadir. Generalisability of fetal ultrasound deep learning models to low-resource imaging settings
 765 in five african countries. *Scientific Reports*, 13(1):2728, Feb 2023. ISSN 2045-2322. doi: 10.1038/
 766 s41598-023-29490-3. URL <https://doi.org/10.1038/s41598-023-29490-3>.

767 Wei Shao and Wayne Brisbane. Micro-ultrasound prostate segmentation dataset, January 2024. URL
 768 <https://doi.org/10.5281/zenodo.10475293>.

769 Harshita Sharma, Lior Drukker, Aris T. Papageorgiou, and J. Alison Noble. Machine learning-based analysis
 770 of operator pupillary response to assess cognitive workload in clinical ultrasound imaging. *Computers in*
 771 *Biology and Medicine*, 135:104589, 2021. ISSN 0010-4825. doi: <https://doi.org/10.1016/j.combiomed.2021.104589>. URL <https://www.sciencedirect.com/science/article/pii/S0010482521003838>.

774 Piyush Sharma, Nan Ding, Sebastian Goodman, and Radu Soricut. Conceptual Captions: A cleaned,
 775 hypernymed, image alt-text dataset for automatic image captioning. In *Proceedings of the 56th Annual*
 776 *Meeting of the Association for Computational Linguistics (Volume 1: Long Papers)*, pp. 2556–2565, 2018.

777 Matthew Shun-Shin. The imperial ai echocardiography dataset. <https://unityimaging.net>, 2023. An
 778 open-access dataset of over 7500 expert-labeled echocardiographic images for AI development in cardiology.
 779 IRAS: 279328, REC: 20/SC/0386. Accessed May 2025.

780 Rohit Singla, Cailin Ringstrom, Grace Hu, Victoria Lessoway, Janice Reid, Christopher Nguan, and Robert
 781 Rohling. The open kidney ultrasound data set. In Bernhard Kainz, Alison Noble, Julia Schnabel, Bishesh
 782 Khanal, Johanna Paula Müller, and Thomas Day (eds.), *Simplifying Medical Ultrasound*, pp. 155–164,
 783 Cham, 2023. Springer Nature Switzerland. ISBN 978-3-031-44521-7.

785 Sithursan Sivasubramaniam, Cedric Osei-Akoto, Yi Zhang, Kurt Stockinger, and Jonathan Fürst.
 786 Sm3-text-to-query: Synthetic multi-model medical text-to-query benchmark. In A. Globerson,
 787 L. Mackey, D. Belgrave, A. Fan, U. Paquet, J. Tomczak, and C. Zhang (eds.), *Advances in Neural Information Processing Systems*, volume 37, pp. 88627–88663. Curran Associates, Inc., 2024. URL https://proceedings.neurips.cc/paper_files/paper/2024/file/a182a8e6ebc91728b6e6b6382c9f7b1e-Paper-Datasets_and_Benchmarks_Track.pdf.

791 Liangtai Sun, Yang Han, Zihan Zhao, Da Ma, Zhennan Shen, Baocai Chen, Lu Chen, and Kai Yu. Sci-
 792 Eval: A multi-level large language model evaluation benchmark for scientific research. *arXiv preprint*
 793 *arXiv:2308.13149*, 2023.

794 Google Team. Advancing multimodal medical capabilities of gemini. *CoRR*, abs/2405.03162, 2024.

796 Abhishek Tyagi, Abhay Tyagi, Manpreet Kaur, Richa Aggarwal, Kapil D. Soni, Jayanthi Sivaswamy, and
 797 Anjan Trikha. Nerve block target localization and needle guidance for autonomous robotic ultrasound
 798 guided regional anesthesia, 2024. URL <https://arxiv.org/abs/2308.03717>.

799 Thomas L. A. van den Heuvel, Dagmar de Bruijn, Chris L. de Korte, and Bram van Ginneken. Automated
 800 measurement of fetal head circumference using 2d ultrasound images, July 2018. URL <https://doi.org/10.5281/zenodo.1327317>.
 801

802 S. Vitale, J. I. Orlando, E. Iarussi, and I. Larrabide. Improving realism in patient-specific abdominal ultrasound
 803 simulation using cyclegans. *International Journal of Computer Assisted Radiology and Surgery*, 15(2):
 804 183–192, February 2020. doi: 10.1007/s11548-019-02046-5. Epub 2019 Aug 7.
 805

806 Qianye Wang, Yipeiand Yang, Lior Drukker, Aris Papageorgiou, Yipeng Hu, and J. Alison Noble. Task
 807 model-specific operator skill assessment in routine fetal ultrasound scanning. *International Journal
 808 of Computer Assisted Radiology and Surgery*, 17(8):1437–1444, Aug 2022. ISSN 1861-6429. doi:
 809 10.1007/s11548-022-02642-y. URL <https://doi.org/10.1007/s11548-022-02642-y>.
 810

811 Xiaoxuan Wang, Ziniu Hu, Pan Lu, Yanqiao Zhu, Jieyu Zhang, Satyen Subramaniam, Arjun R Loomba,
 812 Shichang Zhang, Yizhou Sun, and Wei Wang. SciBench: Evaluating college-level scientific problem-
 813 solving abilities of large language models. *arXiv preprint arXiv:2307.10635*, 2023.
 814

815 Nina Wiedemann, Dianne de Korte-de Boer, Matthias Richter, Sjors van de Weijer, Charlotte Buhre, Franz
 816 A. M. Eggert, Sophie Aarnoudse, Lotte Grevendonk, Steffen Röber, Carlijn M.E. Remie, Wolfgang Buhre,
 817 Ronald Henry, and Jannis Born. Covid-blues - a prospective study on the value of ai in lung ultrasound
 818 analysis. *IEEE Journal of Biomedical and Health Informatics*, pp. 1–12, 2025. doi: 10.1109/JBHI.2025.
 3543686.
 819

820 Untari Novia Wisesty, Irba Fairuz Thufailah, Ria May Dewi, Adiwijaya, and Jondri. Study of segmentation
 821 technique and stereology to detect pco follicles on usg images. *Journal of Computer Science*, 14(3):
 822 351–359, Mar 2018. doi: 10.3844/jcssp.2018.351.359. URL <https://thescipub.com/abstract/jcssp.2018.351.359>.
 823

824 Chaoyi Wu, Xiaoman Zhang, Ya Zhang, Yanfeng Wang, and Weidi Xie. Towards generalist foundation model
 825 for radiology by leveraging web-scale 2d&3d medical data, 2023a. URL <https://arxiv.org/abs/2308.02463>.
 826

827 Chaoyi Wu, Xiaoman Zhang, Ya Zhang, Yanfeng Wang, and Weidi Xie. Towards Generalist Foundation
 828 Model for Radiology by Leveraging Web-scale 2D&3D Medical Data, November 2023b. URL <http://arxiv.org/abs/2308.02463>. arXiv:2308.02463 [cs].
 829

830 Peng Xia, Ze Chen, Juanxi Tian, Yangrui Gong, Ruibo Hou, Yue Xu, Zhenbang Wu, Zhiyuan Fan, Yiyang
 831 Zhou, Kangyu Zhu, Wenhao Zheng, Zhaoyang Wang, Xiao Wang, Xuchao Zhang, Chetan Bansal, Marc
 832 Niethammer, Junzhou Huang, Hongtu Zhu, Yun Li, Jimeng Sun, Zongyuan Ge, Gang Li, James Zou,
 833 and Huaxiu Yao. Cares: A comprehensive benchmark of trustworthiness in medical vision language
 834 models. In A. Globerson, L. Mackey, D. Belgrave, A. Fan, U. Paquet, J. Tomczak, and C. Zhang
 835 (eds.), *Advances in Neural Information Processing Systems*, volume 37, pp. 140334–140365. Curran
 836 Associates, Inc., 2024. URL https://proceedings.neurips.cc/paper_files/paper/2024/file/fde7f40f8ced5735006810534dc66b33-Paper-Datasets_and_Benchmarks_Track.pdf.
 837

838 Xiaolong Xiao, Jianfeng Zhang, Yuan Shao, Jialong Liu, Kaibing Shi, Chunlei He, and Dexing Kong. Deep
 839 learning-based medical ultrasound image and video segmentation methods: Overview, frontiers, and
 840 challenges. *Sensors*, 25(8), 2025. ISSN 1424-8220. doi: 10.3390/s25082361. URL <https://www.mdpi.com/1424-8220/25/8/2361>.
 841

842 XiaohuMini. Xiaohumini. *XiaohuMini News*, January 2025. URL <https://xiaohumini.site>.
 843

844 Qiantong Xu, Fenglu Hong, Bo Li, Changran Hu, Zhengyu Chen, and Jian Zhang. On the tool manipulation
 845 capability of open-source large language models. *arXiv preprint arXiv: 2305.16504*, 2023.

846 Weiwen Xu, Hou Pong Chan, Long Li, Mahani Aljunied, Ruifeng Yuan, Jianyu Wang, Chenghao Xiao,
 847 Guizhen Chen, Chaoqun Liu, Zhaodonghui Li, et al. Lingshu: A generalist foundation model for unified
 848 multimodal understanding and reasoning. *arXiv preprint arXiv:2506.07044*, 2025.

849

850 An Yang, Baosong Yang, Binyuan Hui, Bo Zheng, Bowen Yu, Chang Zhou, Chengpeng Li, Chengyuan Li,
 851 Dayiheng Liu, Fei Huang, et al. Qwen2 technical report. *arXiv preprint arXiv:2407.10671*, 2024.

852

853 Kaining Ying, Fanqing Meng, Jin Wang, Zhiqian Li, Han Lin, Yue Yang, Hao Zhang, Wenbo Zhang, Yuqi Lin,
 854 Shuo Liu, Jiayi Lei, Quanfeng Lu, Runjian Chen, Peng Xu, Renrui Zhang, Haozhe Zhang, Peng Gao, Yali
 855 Wang, Yu Qiao, Ping Luo, Kaipeng Zhang, and Wenqi Shao. Mmt-bench: A comprehensive multimodal
 856 benchmark for evaluating large vision-language models towards multitask agi, 2024.

857

858 Sheng Zhang, Yanbo Xu, Naoto Usuyama, Jaspreet Bagga, Robert Tinn, Sam Preston, Rajesh Rao, Mu Wei,
 859 Naveen Valluri, Cliff Wong, Matthew P. Lungren, Tristan Naumann, and Hoifung Poon. Large-scale
 860 domain-specific pretraining for biomedical vision-language processing. *CoRR*, abs/2303.00915, 2023.

861

862 Tianyi Zhang*, Varsha Kishore*, Felix Wu*, Kilian Q. Weinberger, and Yoav Artzi. Bertscore: Evaluating
 863 text generation with bert. In *International Conference on Learning Representations*, 2020. URL <https://openreview.net/forum?id=SkeHuCVFDr>.

864

865 Wanjun Zhong, Ruixiang Cui, Yiduo Guo, Yaobo Liang, Shuai Lu, Yanlin Wang, Amin Saied, Weizhu Chen,
 866 and Nan Duan. Agieval: A human-centric benchmark for evaluating foundation models, 2023.

867

868 Deyao Zhu, Jun Chen, Xiaoqian Shen, Xiang Li, and Mohamed Elhoseiny. MiniGPT-4: Enhancing vision-
 869 language understanding with advanced large language models. *arXiv preprint arXiv:2304.10592*, 2023.

870

871 Jinguo Zhu, Weiyun Wang, Zhe Chen, Zhaoyang Liu, Shenglong Ye, Lixin Gu, Hao Tian, Yuchen Duan,
 872 Weijie Su, Jie Shao, Zhangwei Gao, Erfei Cui, Xuehui Wang, Yue Cao, Yangzhou Liu, Xinguang Wei,
 873 Hongjie Zhang, Haomin Wang, Weiye Xu, Hao Li, Jiahao Wang, Nianchen Deng, Songze Li, Yinan He,
 874 Tan Jiang, Jiapeng Luo, Yi Wang, Conghui He, Botian Shi, Xingcheng Zhang, Wenqi Shao, Junjun He,
 875 Yingtong Xiong, Wenwen Qu, Peng Sun, Penglong Jiao, Han Lv, Lijun Wu, Kaipeng Zhang, Huipeng
 876 Deng, Jiaye Ge, Kai Chen, Limin Wang, Min Dou, Lewei Lu, Xizhou Zhu, Tong Lu, Dahua Lin, Yu Qiao,
 877 Jifeng Dai, and Wenhui Wang. Internvl3: Exploring advanced training and test-time recipes for open-source
 878 multimodal models, 2025. URL <https://arxiv.org/abs/2504.10479>.

879

880

881

882

883

884

885

886

887

888

889

890

891

892

893 APPENDICES
894

895 Within this supplementary material, we elaborate on the following aspects:
896

897 Appendix A: More Related Work and Future Work
898

899 Appendix B: Safeguarding
900

901 Appendix C: More Evaluation Details
902

903 Appendix D: Prompt Details
904

905 Appendix E: Dataset Details and License
906

907 **USAGE OF LLM**
908

909 LLMs were used in this work as a writing and editing assistant. Specifically, they helped polish the language
910 of the manuscript for clarity and conciseness, suggested alternative phrasings, and formatted some LaTeX
911 tables. LLMs were not used for research ideation or experimental design, but were used to assist coding and
912 prompt design.
913

914

915

916

917

918

919

920

921

922

923

924

925

926

927

928

929

930

931

932

933

934

935

936

937

938

939

940 **A LIMITATIONS AND FUTURE WORK**941 **A.1 MORE RELATED WORK**

944 **Ultrasound Foundation Models.** Several ultrasound-specific models such as USFM (Jiao et al., 2024),
 945 UltraSAM (Meyer et al., 2024), and EchoFM (Kim et al., 2024) pretrain visual backbones using self-
 946 supervised or segmentation-oriented objectives. BiomedCLIP (Zhang et al., 2023), Fetal-CLIP (Maani
 947 et al., 2025), and EchoCLIP (Christensen et al., 2024) explore vision-language pretraining in biomedical
 948 domains, but are often narrow in scope (e.g., fetal or cardiac imaging only), require fine-tuning, and lack the
 949 general-purpose zero-shot capabilities of LVLMs. Our benchmark evaluates generalist LVLMs directly, across
 950 a diverse range of ultrasound tasks, without task-specific adaptation. Table 4 gives a detailed comparison of
 951 existing benchmarks and datasets.

952 Table 4: Comparison of U2-BENCH with existing benchmarks and foundation model datasets.
 953

954 Dataset / Benchmark	#Tasks	#Anatomies	#Val US Cases	Multimodal	Free-text Output	Public Available
955 USFM (Jiao et al., 2024)	3	12	22,421	✗	✗	✗
956 UltraSam (Meyer et al., 2024) [†]	2	58	14,000	✗	✗	✓
957 FetalCLIP (Maani et al., 2025)	4	Fetal	-	✓	✗	✗
958 EchoCLIP (Christensen et al., 2024)	5	Cardiac	21,484	✓	✓	✗
959 EchoFM (Kim et al., 2024)	4	Cardiac	-	✗	✗	✗
960 GMAI-MMBench (Chen et al., 2024a)*	2	5	~ 1,800	✓	✗	✓
U2-BENCH (Ours)						
961	8	15	7,241	✓	✓	✓

961 [†]UltraSam’s US-43d is composed of public datasets, but not released as a unified benchmark.

962 * We only count the statistics of the ultrasound part of the GMAI-MMBench dataset for a fair comparison.

963 **A.2 LIMITATIONS**

964 **Ethical and Applicability Considerations.** U2-BENCH is designed as a research-oriented benchmark and
 965 is not intended for clinical deployment or diagnostic decision-making. Any real-world application of models
 966 evaluated on this benchmark would require separate validation and regulatory approval. Although all data
 967 sources are licensed or publicly available and de-identified where applicable, we acknowledge that not all
 968 ethical and demographic dimensions of fairness can be fully accounted for at this stage.

969 **Evaluation Scope.** The benchmark focuses on key task categories relevant to ultrasound interpretation—such as anatomical recognition, diagnostic classification, and structured report generation. While these
 970 tasks are representative and grounded in clinical utility, they do not exhaust the full landscape of sonographic
 971 applications. The evaluation metrics used (e.g., accuracy, BLEU) may not capture the full subtlety of expert
 972 clinical judgment, especially in edge cases.

973 **Ultrasound-Specific Challenges.** Ultrasound imaging is highly operator-dependent and subject to artifacts
 974 such as shadowing, speckle, and angle variation. Variability in scanning protocols and lack of standardized
 975 definitions (e.g., for “standard planes”) can complicate model training and evaluation. These modality-specific
 976 challenges are inherent to ultrasound and reflect real-world complexities rather than flaws in the benchmark
 977 design.

978 **A.3 FUTURE WORK**

979 **Extending Dataset Diversity and Robustness.** While U2-BENCH aggregates data from a broad range
 980 of sources, further expansion to include more institutions, device types, and global populations would

987 improve its representativeness. Future iterations of the benchmark will explore domain adaptation, adversarial
988 robustness, and performance under distribution shifts to better simulate deployment conditions in varied
989 clinical environments.
990

991 **Model Generalization and Multimodal Reasoning.** Current LVLMs still struggle with fine-grained spatial
992 tasks, consistency across subgroups, and robust generation of clinically meaningful language. In future work,
993 we aim to incorporate richer contextual information (e.g., patient history, multi-view inputs) to better assess
994 models' multimodal integration capabilities and real-world reasoning performance.
995

996 **Video-Based and Real-Time Evaluation.** U2-BENCH currently operates on frame-based inputs to ensure
997 comparability across models. However, clinical ultrasound interpretation often involves dynamic, probe-
998 controlled acquisition. Extending the benchmark to include video sequences, real-time tasks, and longitudinal
999 case studies will be a major step toward closing the simulation-to-clinic gap.
1000

1001 **Theoretical Foundations and Causality.** Our current benchmark is designed for practical performance
1002 evaluation. Future work will incorporate diagnostic reasoning audits, causal probing methods, and uncertainty
1003 quantification frameworks to deepen our understanding of LVLM behavior in high-stakes medical applications.
1004

1005 **Standardization in Ultrasound AI.** There is a growing need for community consensus on annotation
1006 standards, task definitions, and evaluation protocols in ultrasound AI. We hope U2-BENCH can serve as a
1007 starting point for these conversations and will actively evolve in response to feedback from both clinical and
1008 technical communities.
1009
1010
1011
1012
1013
1014
1015
1016
1017
1018
1019
1020
1021
1022
1023
1024
1025
1026
1027
1028
1029
1030
1031
1032
1033

1034 **Table 5: Summary of annotated datasets used in U2-BENCH, grouped by core capability and task.** The
 1035 “Case Number” column indicates the number of samples per task, while “Total” reflects the overall count
 1036 when available. More details about the datasets are included in Appendix E.

1038 Capability	1038 Task	1038 Case Number	1038 Source Dataset	1038 Total
1039 Classification	1040 DD	1,411	Breast Lesion Detection in Ultrasound Videos (Lin et al., 2022); Breast Ultrasound Images Dataset (Al-Dhabayani et al., 2020); Dermatologic Ultrasound Images for classification (Laverde Saad et al., 2021); Knee ultrasound dataset in a population-based cohort (Novin et al., 2023); KFGNet (NeuronXITU & palkia1998, 2023); GDPHSYSUCC (Mo et al., 2022); LEPSet (Li et al., 2023b); COVID-BLUES (Wiedemann et al., 2025); Ultrasound Guided Regional Anesthesia (Tyagi et al., 2024); Ultrasound Breast Images for Breast Cancer (Sairam, 2020); Algerian Ultrasound Images Thyroid Dataset: AUTTD (Maroua, 2020); Auto-PCOS classification (Divekar & Sonawane, 2024)	2,999
			FETAL PLANES DB (Burgos-Artizu et al., 2020); FPUS23 (Prabakaran et al., 2023); CAMUS (Leclerc et al., 2019); Knee ultrasound dataset in a population-based cohort (Novin et al., 2023); Thyroid (Krönke et al., 2022); ACOUSLIC-AI (Sappia, 2024); JNU-IFM (Lu et al., 2022); Carotid Artery Ultrasound and Color Doppler (Pahuni Choudhary, 2023); Auto-PCOS classification (Maroua, 2020); African Fetal Standard Plane (Sendra-Balcells et al., 2023); DDTI (Pedraza et al., 2015); CAMUS (Leclerc et al., 2019); CUBS (Meiburger et al., 2021); COVID-BLUES (Wiedemann et al., 2025); Dataset of B-mode fatty liver ultrasound images (Byra et al., 2018); The Open Kidney Ultrasound Dataset (Singla et al., 2023); Micro-Ultrasound Prostate Segmentation Dataset (Shao & Brisbane, 2024); Breast Ultrasound Images Dataset (Al-Dhabayani et al., 2020); Knee ultrasound dataset in a population-based cohort (Novin et al., 2023); Polycystic Ovary Ultrasound Images Dataset (Wisesty et al., 2018)	
	VRA	1,588	FETAL PLANES DB (Burgos-Artizu et al., 2020); FPUS23 (Prabakaran et al., 2023); CAMUS (Leclerc et al., 2019); Knee ultrasound dataset in a population-based cohort (Novin et al., 2023); Thyroid (Krönke et al., 2022); ACOUSLIC-AI (Sappia, 2024); JNU-IFM (Lu et al., 2022); Carotid Artery Ultrasound and Color Doppler (Pahuni Choudhary, 2023); Auto-PCOS classification (Maroua, 2020); African Fetal Standard Plane (Sendra-Balcells et al., 2023); DDTI (Pedraza et al., 2015); CAMUS (Leclerc et al., 2019); CUBS (Meiburger et al., 2021); COVID-BLUES (Wiedemann et al., 2025); Dataset of B-mode fatty liver ultrasound images (Byra et al., 2018); The Open Kidney Ultrasound Dataset (Singla et al., 2023); Micro-Ultrasound Prostate Segmentation Dataset (Shao & Brisbane, 2024); Breast Ultrasound Images Dataset (Al-Dhabayani et al., 2020); Knee ultrasound dataset in a population-based cohort (Novin et al., 2023); Polycystic Ovary Ultrasound Images Dataset (Wisesty et al., 2018)	
1042 Detection	1043 OD	1,918	DDTI (Pedraza et al., 2015); Micro-Ultrasound Prostate Segmentation Dataset (Shao & Brisbane, 2024); Breast Ultrasound Images Dataset (Al-Dhabayani et al., 2020); KFGNet (NeuronXITU & palkia1998, 2023); BrEaST (Pawlowska et al., 2024)	2,921
			The Open Kidney Ultrasound Dataset (Singla et al., 2023); Echogenic (Da Correggio et al., 2023); FALLMUD (FALLMUD); CAMUS (Leclerc et al., 2019); HC18 (van den Heuvel et al., 2018); Thyroid (Krönke et al., 2022); CCA (Bi et al., 2024); Ultrasound Guided Regional Anesthesia (Tyagi et al., 2024); C-TRUS Dataset (Leenings et al., 2025); ACOUSLIC-AI (Sappia, 2024); PSFHS (Bai, 2024); JNU-IFM (Lu et al., 2022); US simulation & segmentation (Vitale et al., 2020)	
	KD	500	Unity Imaging Collaborative (Shun-Shin, 2023)	
1046 Regression	CVE	521	CAMUS (Leclerc et al., 2019); CUBS (Meiburger et al., 2021); HC18 (van den Heuvel et al., 2018); ACOUSLIC-AI (Sappia, 2024); Dataset of B-mode fatty liver ultrasound images (Byra et al., 2018)	521
1047 Generation	RG	600	Chinese Ultrasound Report Dataset (Li et al., 2024)	800
1048	CG	200	FPUS23 (Prabakaran et al., 2023)	
1049				Overall Total 7,241

1054 B SAFEGUARDING

1055 This study involves secondary use of de-identified, publicly available or licensed ultrasound datasets for the
 1056 purpose of benchmarking machine learning models. All data used in **U2-BENCH** are either publicly released
 1057 with appropriate usage permissions or obtained through official licensing agreements. No personally identifiable
 1058 information is used, and all experiments are conducted in accordance with relevant data protection and
 1059 ethical guidelines. Human annotators involved in quality assurance were trained to follow data confidentiality
 1060 protocols, and no clinical decision-making was involved at any stage of this work.

1063 C MORE EVALUATION DETAILS

1066 C.1 DATASETS USED

1067 In Table 5.

1069 C.2 EXPERIMENT SETTING

1070 We conducted experiments on **U2-BENCH** with both open-source and closed-source LVLMs. Uniform
 1071 prompts were applied across all models. The evaluation was executed on 32 NVIDIA A800 GPUs over a
 1072 period of approximately two weeks, using the OpenCompass VLMEvalKit (Duan et al., 2024), with additional
 1073 support from a unified framework (XiaohuMini, 2025). [All models were tested with temperature 0.7](#).

1074 **Evaluated Models.** We evaluated 23 LVLMs, spanning both open-source and closed-source systems, and
 1075 including both general-purpose and medical-specialized variants.

- 1079 • **Qwen2.5-VL Series (Yang et al., 2024):** This includes *Qwen2.5-VL-3B-Instruct*, *Qwen2.5-VL-7B-Instruct*, *Qwen2.5-VL-32B-Instruct*, *Qwen2.5-VL-72B-Instruct*

- **Medical-Specific Open-Source Models:** *MiniGPT-Med* (Wu et al., 2023b), *MedDr* (He et al., 2024), *Lingshu*, *MedGemma-4B* (Anil et al., 2023).
- **Other Open-Source Models:** *Phi-4-Multimodal-Instruct-5.6B* (Abdin et al., 2024), *InternVL3-9B-Instruct* (Zhu et al., 2025), *LLaVA-1.5-13B* (Liu et al., 2023a), *Mistral-Small-3.1-24B-Instruct-2503* (Jiang et al., 2023), *DeepSeek-VL2* (DeepSeek-AI, 2024)
- **Closed-Source Models:** *GPT-4o-Mini*, *GPT-4o-2024-08-06* (OpenAI, 2023), *GPT-5*, *Gemini-1.5-Pro (exp-02-05)*, *Gemini-2-Pro (exp-02-05)*, *Gemini-2.5-Pro-Preview (exp-02-05)* (Anil et al., 2023), *Claude-3-Sonnet (20250219)* (Anthropic, 2024), *Qwen-Max-2025-01-25* (Bai et al., 2023a), *Doubaoo-1.5-Vision-Pro-32K-250115* (ByteDance, 2024), *Dolphin-V1* (Model developed by *Dolphin AI*)
- **Random Guessing:** implemented by uniformly sampling from the valid answer set for each classification task.

1098 C.3 JUSTIFICATION OF U2-SCORE WEIGHTING

1100 **Table 6: Task-specific evaluation metrics and weights.** The corresponding weight w_t and metric used for
1101 overall score aggregation for each task.

t	1	2	3	4	5	6	7	8
	DD	VRA	LL	OD	KD	CVE	RG	CG
w_t	0.2	0.2	0.07	0.27	0.07	0.07	0.08	0.04
d_t	Acc.	Acc.	Acc.	Acc.	Acc.	1-RMSE	BLEU-4	BLEU-4

1107 The U2-Score summarizes model performance across the eight benchmark tasks in **U2-BENCH** through a
1108 weighted aggregation:

$$1109 \text{U2-Score} := \sum_{t=1}^N w_t \cdot d_t, \quad \text{where} \quad w_t = \frac{n_t}{\sum_j n_j}, \quad d_t \in [0, 1] \quad (2)$$

1113 Each task t is associated with a weight w_t proportional to its number of annotated examples n_t , and a
1114 normalized evaluation score d_t representing performance on that task. This formulation ensures that the final
1115 score reflects both task competence and dataset composition.

1116 The weighting design of U2-Score is rooted in data-driven representation of ultrasound practice. All bench-
1117 mark tasks are constructed from licensed and publicly available datasets sourced through a comprehensive
1118 and systematic search. As a result, the sample distribution across tasks captures the structure of real-world
1119 ultrasound data availability and usage. Tasks with greater sample counts typically correspond to more
1120 standardized, clinically widespread, and institutionally supported workflows—such as disease diagnosis and
1121 view recognition. Conversely, tasks with fewer examples often reflect more specialized applications or less
1122 frequently annotated modalities.

1123 By aligning task weights with dataset size, the U2-Score encodes the practical significance and maturity
1124 of each task in the public ultrasound domain. This approach also promotes reliable aggregate evaluation,
1125 as scores are more robustly informed by tasks with greater data coverage. The resulting metric balances
1126 comprehensiveness with grounded applicability, supporting fair and reproducible model comparison in the
1127 current landscape of ultrasound AI research.

1128

C.4 ERROR ANALYSIS

1129

1130

1131

1132

1133

1134

1135

1136

1137

1138

1139

1140

1141

Diagnosis Task (DD)

Accuracy: 0.05 (1/20 models correct)

Reference Answer: 4A

Model Responses:

- **gemini-2.5-pro-preview-03-25:** 5
- **Do-3B:** 2
- **gpt-4o-2024-08-06:** '3'
- **doubao-1.5-vision-pro-32k-250115:** Insufficient information provided to determine BI - RADS category. Please describe the sonographic characteristics of the lesion in the image.
- **MedDr:** 5
- **qwen-max-2025-01-25:** 3
- **local_model:** 2
- **claude-3-7-sonnet-20250219:** 4C
- **gemini-2.0-pro-exp-02-05:** 4C
- **deepseek-v12:** 4B
- **qwen2.5-vl-3b-instruct:** 2
- **Qwen2.5-VL-7B-Instruct-Pro:** 4A
- **gemini-1.5-pro-latest:** 2
- **Qwen2.5-VL-32B-Instruct:** 4B
- **InternVL3-9B-Instruct:** 4B
- **Phi-4-multimodal-instruct:** I cannot synthesize the sonographic characteristics of the lesions or make a BI-RADS assessment without the actual ultrasound images or a detailed description of the findings. If you provide the relevant details or images, I would be able to assist you with the assessment.
- **LLaVA-1.5-13B-HF:** '2'
- **Mistral-Small-3.1-24B-Instruct-2503:** 3
- **Do-7B:** The anatomical component most vividly portrayed is the breast.
- **gpt-4o-mini:** 2

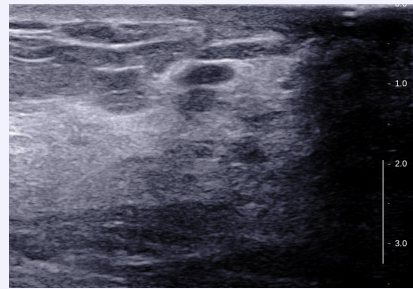


Figure 4: Ultrasound image for Diagnosis Task 40: case001273

Prompt: You are a radiologist analyzing a breast ultrasound image. Your task is to synthesize the sonographic characteristics of any identified lesions (or lack thereof) into a final ACR BI-RADS (Breast Imaging Reporting and Data System) assessment category.

BI-RADS Ultrasound Assessment Category Definitions

- '2' (Benign): Findings are definitively benign (e.g., simple cysts, intramammary lymph nodes, stable surgical implants/changes). 0% likelihood of malignancy. Requires routine screening follow-up.
- '3' (Probably Benign): Findings have characteristic benign features but are not definitively benign (e.g., presumed fibroadenoma, complicated cyst). Very low likelihood of malignancy (<2%). Short-interval (e.g., 6-month) follow-up is typically recommended.
- '4A' (Low Suspicion for Malignancy): Findings warrant biopsy but have a low probability of malignancy (<2% to \leq 10%).
- '4B' (Moderate Suspicion for Malignancy): Findings warrant biopsy with an intermediate probability of malignancy (<10% to \leq 50%).
- '4C' (High Suspicion for Malignancy): Findings warrant biopsy with high probability of malignancy (>50% to \geq 95%), without the classic features of Category 5.
- '5' (Highly Suggestive of Malignancy): Findings have classic malignant features (e.g., irregular spiculated mass). Very high probability of malignancy (\geq 95%). Biopsy is required, and definitive action should be taken regardless of pathology results if discordant.

Choose the single most appropriate BI-RADS assessment category from the options below.
options: ['2', '3', '4A', '4B', '4C', '5']

Output format: only the exact text of the chosen option from the list above. Do not include any introductory phrases, explanations, numbering, or formatting.

1175
 1176
 1177
 1178
 1179
 1180
 1181
 1182
 1183
 1184
 1185
 1186
 1187
 1188
 1189
 1190
 1191
 1192
 1193
 1194
 1195
 1196
 1197
 1198
 1199
 1200
 1201
 1202
 1203
 1204
 1205
 1206
 1207
 1208
 1209
 1210
 1211
 1212
 1213
 1214
 1215
 1216
 1217
 1218
 1219
 1220
 1221

View Recognition and Assessment Tasks (VRA)



Reference Answer: hdvb

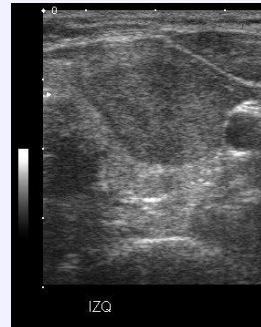
Model Responses:

- **Random Guessing:** huvf
- **MiniGPT-Med:** hdvf
- **MedDr:** hdvb
- **Qwen-2.5-VL-3B-Instruct:** hdvf
- **Qwen-2.5-VL-7B-Instruct:** hdvb
- **Qwen-2.5-VL-32B-Instruct:** hdvb
- **Qwen-2.5-VL-72B-Instruct:** hdvb
- **DeepSeek-VL2:** hdvf
- **InternVL3-9B-Instruct:** hdvf
- **LLaVA-1.5-13B:** huvb
- **Phi-4-Multimodal-Instruct:** hdvf
- **Mistral-Small-3.1-24B-Inst.:** hdvb
- **Doubaol-1.5-Vision-Pro-32k:** hdvb
- **GPT-4o-Mini:** hdvf
- **GPT-4o:** hdvb
- **Gemini-1.5-Pro:** hdvf
- **Gemini-2.0-Pro-Exp:** hdvb
- **Gemini-2.5-Pro-Preview:** hdvf
- **Claude-3.7-Sonnet:** huvb
- **Qwen-Max:** hdvb
- **Dolphin-V1:** hdvb

Prompt: You are a radiologist analyzing a fetal ultrasound image. Your task is to determine the fetal presentation and orientation based on the provided ultrasound image. Specifically, identify whether the fetal head is down(hd) or up(hu). Additionally, determine if the fetal back is primarily oriented towards the ultrasound probe (vb) or towards the ultrasound probe (vf). Choose the single best option from the options below that accurately combines these findings. options: 'hdvb', 'hdvf', 'huvb', 'huvf' Output format: only the exact text of the chosen option from the list above. Do not include any introductory phrases, explanations, numbering, or formatting.

1222
12231224
1225
1226
1227
1228
1229
1230
1231
1232
1233
1234
1235
1236
1237
1238
1239
1240
1241
1242
1243
1244
1245
1246
1247
1248
1249
1250
1251
1252
1253
1254
1255
1256
1257
1258
1259
1260
1261
1262
1263
1264
1265
1266
1267
1268

Lesion Localization Tasks (LL)



Reference Answer: upper left

Model Responses:

- **Random Guessing:** lower right
- **MiniGPT-Med:** upper center
- **MedDr:** upper left
- **Qwen-2.5-VL-3B-Instruct:** middle left
- **Qwen-2.5-VL-7B-Instruct:** upper left
- **Qwen-2.5-VL-32B-Instruct:** upper left
- **Qwen-2.5-VL-72B-Instruct:** upper left
- **DeepSeek-VL2:** upper right
- **InternVL3-9B-Instruct:** upper center
- **LLaVA-1.5-13B:** middle left
- **Phi-4-Multimodal-Instruct:** upper center
- **Mistral-Small-3.1-24B-Inst.:** upper left
- **Doubao-1.5-Vision-Pro-32k:** upper left
- **GPT-4o-Mini:** upper right
- **GPT-4o:** upper left
- **Gemini-1.5-Pro:** upper right
- **Gemini-2.0-Pro-Exp:** upper left
- **Gemini-2.5-Pro-Preview:** upper right
- **Claude-3.7-Sonnet:** upper center
- **Qwen-Max:** middle left
- **Dolphin-V1:** upper left

Prompt: You are a radiologist analyzing an ultrasound image of thyroid. Your task is to identify the primary location of any visible lesion(s) relative to the boundaries of the displayed image. Consider the lesion's center location or most prominent area when deciding. Choose the single option from the list below that best describes this location, even if the fit is approximate. options: upper left, upper center, upper right, middle left, center, middle right, lower left, lower center, lower right, not visible
Output format: only the exact text of the chosen option from the list above. Do not include any introductory phrases, explanations, numbering, or formatting.

1269
 1270
 1271
 1272
 1273
 1274
 1275
 1276
 1277
 1278
 1279
 1280
 1281
 1282
 1283
 1284
 1285
 1286
 1287
 1288
 1289
 1290
 1291
 1292
 1293
 1294
 1295
 1296
 1297
 1298
 1299
 1300
 1301
 1302
 1303
 1304
 1305
 1306
 1307
 1308
 1309
 1310
 1311
 1312
 1313
 1314
 1315

Organ Detection Tasks (OD)

Reference Answer: center

Model Responses:

- **Random Guessing:** lower left
- **MiniGPT-Med:** middle right
- **MedDr:** center
- **Qwen-2.5-VL-3B-Instruct:** middle right
- **Qwen-2.5-VL-7B-Instruct:** center
- **Qwen-2.5-VL-32B-Instruct:** center
- **Qwen-2.5-VL-72B-Instruct:** center
- **DeepSeek-VL2:** middle left
- **InternVL3-9B-Instruct:** lower center
- **LLaVA-1.5-13B:** middle right
- **Phi-4-Multimodal-Instruct:** middle right
- **Mistral-Small-3.1-24B-Inst.:** center
- **Doubao-1.5-Vision-Pro-32k:** center
- **GPT-4o-Mini:** lower center
- **GPT-4o:** center
- **Gemini-1.5-Pro:** lower center
- **Gemini-2.0-Pro-Exp:** center
- **Gemini-2.5-Pro-Preview:** lower center
- **Claude-3.7-Sonnet:** center
- **Qwen-Max:** middle right
- **Dolphin-V1:** center



Prompt: You are a radiologist analyzing an ultrasound image of liver. Your task is to identify the primary location of the target organ relative to the boundaries of the displayed image. Consider the organ's center location or most prominent area when deciding. Choose the single option from the list below that best describes this location, even if the fit is approximate. options: upper left, upper center, upper right, middle left, center, middle right, lower left, lower center, lower right, not visible
Output format: only the exact text of the chosen option from the list above. Do not include any introductory phrases, explanations, numbering, or formatting.

1316
1317
1318
1319
1320
1321
1322
1323
1324
1325
1326
1327
1328
1329
1330

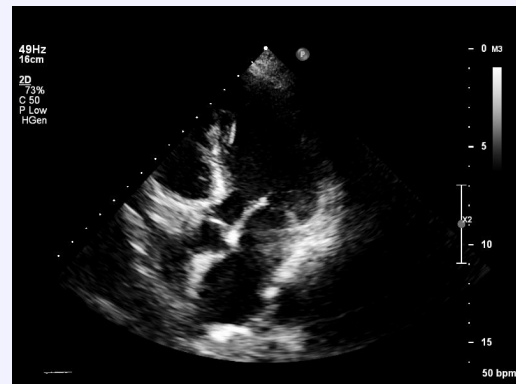
Keypoint Detection Tasks (KD)

1331
1332
1333
1334
1335
1336
1337
1338
1339
1340
1341
1342
1343
1344
1345
1346
1347
1348
1349
1350
1351
1352
1353
1354
1355
1356
1357
1358
1359
1360
1361
1362

Reference Answer: middle right

Model Responses:

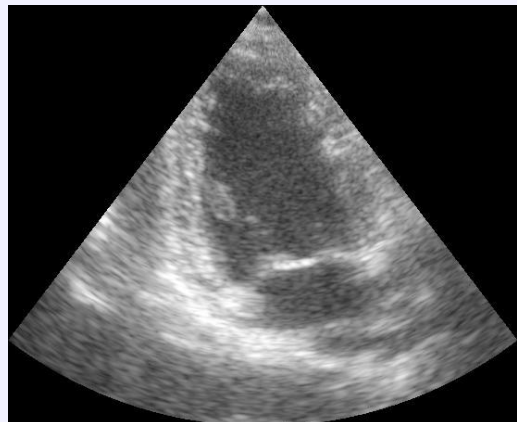
- **Random Guessing:** upper center
- **MiniGPT-Med:** middle left
- **MedDr:** middle right
- **Qwen-2.5-VL-3B-Instruct:** center
- **Qwen-2.5-VL-7B-Instruct:** middle right
- **Qwen-2.5-VL-32B-Instruct:** middle right
- **Qwen-2.5-VL-72B-Instruct:** middle right
- **DeepSeek-VL2:** center
- **InternVL3-9B-Instruct:** middle left
- **LLaVA-1.5-13B:** center
- **Phi-4-Multimodal-Instruct:** lower right
- **Mistral-Small-3.1-24B-Inst.:** middle right
- **Doubao-1.5-Vision-Pro-32k:** middle right
- **GPT-4o-Mini:** center
- **GPT-4o:** middle right
- **Gemini-1.5-Pro:** center
- **Gemini-2.0-Pro-Exp:** middle right
- **Gemini-2.5-Pro-Preview:** center
- **Claude-3.7-Sonnet:** middle right
- **Qwen-Max:** center
- **Dolphin-V1:** middle right



Prompt: You are a radiologist analyzing an ultrasound image of heart. Your task is to identify the primary location of the key anatomical landmark point relative to the boundaries of the displayed image. Consider the landmark's precise position when deciding. Choose the single option from the list below that best describes this location, even if the fit is approximate. options: upper left, upper center, upper right, middle left, center, middle right, lower left, lower center, lower right, not visible
 Output format: only the exact text of the chosen option from the list above. Do not include any introductory phrases, explanations, numbering, or formatting.

1363
1364
1365
1366
1367
1368
1369
1370
1371
1372
1373
1374
1375
1376
1377
1378
1379
1380
1381
1382
1383
1384
1385
1386
1387
1388
1389
1390
1391
1392
1393
1394
1395
1396
1397
1398
1399
1400
1401
1402
1403
1404
1405
1406
1407
1408
1409

Cardiac View Evaluation Tasks (CVE)



Reference Answer: 2CH

Model Responses:

- **Random Guessing:** 4CH
- **MiniGPT-Med:** 4CH
- **MedDr:** 2CH
- **Qwen-2.5-VL-3B-Instruct:** 4CH
- **Qwen-2.5-VL-7B-Instruct:** 4CH
- **Qwen-2.5-VL-32B-Instruct:** 4CH
- **Qwen-2.5-VL-72B-Instruct:** 4CH
- **DeepSeek-VL2:** 4CH
- **InternVL3-9B-Instruct:** 4CH
- **LLaVA-1.5-13B:** 4CH
- **Phi-4-Multimodal-Instruct:** 4CH
- **Mistral-Small-3.1-24B-Inst.:** 4CH
- **Doubaol-1.5-Vision-Pro-32k:** 2CH
- **GPT-4o-Mini:** 4CH
- **GPT-4o:** 4CH
- **Gemini-1.5-Pro:** 4CH
- **Gemini-2.0-Pro-Exp:** 4CH
- **Gemini-2.5-Pro-Preview:** 4CH
- **Claude-3.7-Sonnet:** 2CH
- **Qwen-Max:** 4CH
- **Dolphin-V1:** 2CH

Prompt: You are a radiologist or cardiologist specializing in echocardiography, analyzing an apical view ultrasound image of the human heart. Your task is to accurately identify the specific apical view presented in the provided echocardiogram image. Carefully examine the cardiac structures visible. Determine if the image displays primarily the left ventricle and left atrium only (indicative of a 2-Chamber view, 2CH), or if it clearly shows all four chambers: the left ventricle, right ventricle, left atrium, and right atrium (indicative of a 4-Chamber view, 4CH). Choose the single best option from the list below that correctly identifies the view.

options: 2CH, 4CH

Output format: only the exact text of the chosen option from the list above. Do not include any introductory phrases, explanations, numbering, or formatting.

1410
1411
1412
1413
1414
1415
1416
1417
1418
1419
1420
1421
1422
1423

Cardiac Grading Tasks (CG)

Reference Answer: Moderate OA

Model Responses:

- **Random Guessing:**
- **MiniGPT-Med:** Questionable OA
- **MedDr:** Moderate OA
- **Qwen-2.5-VL-3B-Instruct:** No OA
- **Qwen-2.5-VL-7B-Instruct:** Questionable OA
- **Qwen-2.5-VL-32B-Instruct:** Mild OA
- **Qwen-2.5-VL-72B-Instruct:** Mild OA
- **DeepSeek-VL2:** Questionable OA
- **InternVL3-9B-Instruct:** No OA
- **LLaVA-1.5-13B:** No OA
- **Phi-4-Multimodal-Instruct:** Questionable OA
- **Mistral-Small-3.1-24B-Inst.:** Mild OA
- **Doubao-1.5-Vision-Pro-32k:** Moderate OA
- **GPT-4o-Mini:** No OA
- **GPT-4o:** No OA
- **Gemini-1.5-Pro:** Questionable OA
- **Gemini-2.0-Pro-Exp:** Mild OA
- **Gemini-2.5-Pro-Preview:** Questionable OA
- **Claude-3.7-Sonnet:** Mild OA
- **Qwen-Max:** Mild OA
- **Dolphin-V1:** Moderate OA



Prompt: You are a radiologist analyzing an ultrasound image of left/right knee. Your task is to assess the severity of osteoarthritis (OA) using the established Kellgren-Lawrence (KL) grading system. Kellgren-Lawrence (KL) Grade Mapping to Options:
 •'No OA': Corresponds to KL Grade 0 (No radiographic features of OA).
 •'Questionable OA': Corresponds to KL Grade 1 (Doubtful JSN and possible minute osteophytes).
 •'Mild OA': Corresponds to KL Grade 2 (Definite osteophytes and possible JSN).
 •'Moderate OA': Corresponds to KL Grade 3 (Moderate multiple osteophytes, definite JSN, some sclerosis, possible deformity).
 •'Severe OA': Corresponds to KL Grade 4 (Large osteophytes, marked JSN, severe sclerosis, definite deformity).
 •'Total joint replacement': Indicates the presence of knee arthroplasty components (prosthesis), which replaces the native joint structures evaluated by the KL scale.
 options: 'Mild OA', 'Moderate OA', 'No OA', 'Questionable OA', 'Severe OA', 'Total joint replacement'
 Output format: only the exact text of the chosen option from the list above. Do not include any introductory phrases, explanations, numbering, or formatting.

1457
1458

Report Generation Tasks (RG) Input

1459

1460

1461

1462

1463

1464

1465

1466

1467

1468

1469

1470

1471

1472

1473

1474

1475

1476

1477

1478

1479

1480

1481

1482

1483

1484

1485

1486

1487

1488



1489 *Prompt:* You are a radiologist analyzing an ultrasound image focused on the Liver.

1490 Your task is generate a concise and informative radiological report based strictly on the visual
1491 findings within the provided image. Your report should describe the primary organ's appearance (size,
1492 shape, borders/capsule), its parenchymal echotexture (e.g., homogeneous, heterogeneous,
1493 echogenicity relative to reference structures), and identify any visible abnormalities (e.g., masses,
1494 cysts, fluid collections, calcifications, ductal dilation). Comment on relevant adjacent structures if
1495 visualized. Use standard radiological terminology.

1496 Output format: Strings, that is your report.

1497 Example: The liver morphology is full with a smooth capsule. The parenchymal echotexture is fine
1498 and diffusely increased. Visualization of the portal venous system is suboptimal. Intrahepatic and
1499 extrahepatic bile ducts are not dilated. The main portal vein diameter is within normal limits. The
1500 gallbladder is normal in size and shape. The wall is smooth and not thickened. No obvious abnormal
1501 echoes are seen within the lumen. The pancreas is normal in size and shape with homogeneous
1502 parenchymal echotexture. The pancreatic duct is not dilated. No definite space-occupying lesion is
1503 seen within the pancreas. The spleen is normal in size and shape with homogeneous parenchymal
echotexture. No obvious space-occupying lesion is seen within the spleen.

1504
1505 **Report Generation Tasks (RG) Output**
15061507 **Reference Answer:** The liver morphology is full with a smooth capsule. The parenchymal
1508 echotexture is fine and diffusely increased. Visualization of the portal venous system is suboptimal.
1509 Intrahepatic and extrahepatic bile ducts are not dilated. The main portal vein diameter is within
1510 normal limits. No focal lesions are identified.1511 **Model Responses:**1512

- 1513 • **Random Guessing:**
- 1514 • **MiniGPT-Med:** The liver shows normal size and contour with homogeneous echotexture.
1515 No focal lesions or biliary dilatation noted. Portal structures appear normal.
- 1516 • **MedDr:** The liver demonstrates normal size and contour with a smooth capsule. The
1517 parenchymal echotexture is homogeneous with normal echogenicity. No focal lesions
1518 identified. Intrahepatic biliary ducts are not dilated. Portal venous structures appear normal.
- 1519 • **Qwen-2.5-VL-3B-Instruct:** The liver appears normal in size with a smooth contour. The
1520 parenchymal echotexture is homogeneous without focal lesions. No intrahepatic biliary
1521 dilatation is seen.
- 1522 • **Qwen-2.5-VL-7B-Instruct:** The liver appears normal in size with a smooth capsule. The
1523 parenchymal echotexture is homogeneous with no focal lesions. No intrahepatic or
1524 extrahepatic biliary dilatation is seen. The portal venous structures appear normal.
- 1525 • **Qwen-2.5-VL-32B-Instruct:** The liver appears normal in size with a smooth contour. The
1526 parenchymal echotexture is homogeneous with normal echogenicity. No focal lesions such
1527 as masses, cysts, or calcifications are identified. The intrahepatic bile ducts are not dilated.
1528 The portal venous structures appear normal. No perihepatic fluid collection is observed.
- 1529 • **Qwen-2.5-VL-72B-Instruct:** The liver demonstrates normal size and contour with a smooth
1530 capsule. The parenchymal echotexture is homogeneous with normal echogenicity. No focal
1531 lesions or masses are identified. The intrahepatic biliary tree is not dilated. Portal venous
1532 structures appear normal. No perihepatic fluid collection is seen.
- 1533 • **DeepSeek-VL2:** The liver appears normal in size with a smooth contour. The parenchymal
1534 echotexture is homogeneous with normal echogenicity. No focal lesions are identified. The
1535 intrahepatic bile ducts are not dilated. The portal venous structures appear normal. No
1536 perihepatic fluid collection is observed.
- 1537 • **InternVL3-9B-Instruct:** The liver appears normal in size with a smooth contour. The
1538 parenchymal echotexture is homogeneous without focal lesions. No intrahepatic or
1539 extrahepatic biliary dilatation is seen. The portal venous structures appear normal.
- 1540 • **LLaVA-1.5-13B:** The liver appears normal in size with a smooth contour. The parenchymal
1541 echotexture is homogeneous without focal lesions. No intrahepatic biliary dilatation is seen.
1542 The portal structures appear normal.
- 1543 • **Phi-4-Multimodal-Instruct:** The liver appears normal in size with a smooth contour. The
1544 parenchymal echotexture is homogeneous with no focal lesions. No intrahepatic or
1545 extrahepatic biliary dilatation is seen. The hepatic vessels appear normal.
- 1546 • **Mistral-Small-3.1-24B-Inst.:** The liver demonstrates normal size and contour with a
1547 smooth capsule. The parenchymal echotexture is homogeneous with normal echogenicity.
1548 No focal lesions or masses are identified. The intrahepatic biliary tree is not dilated. Portal
1549 venous structures appear normal.

- **Doubao-1.5-Vision-Pro-32k:** The liver appears normal in size with a smooth contour. The parenchymal echotexture is homogeneous with normal echogenicity. No focal lesions are identified. The intrahepatic bile ducts are not dilated. The portal venous structures appear normal.
- **GPT-4o-Mini:** The liver appears normal in size with a smooth contour. The parenchymal echotexture is homogeneous without focal lesions. No intrahepatic or extrahepatic biliary dilatation is seen. The hepatic vessels appear normal. No ascites or other abnormalities are identified in the visualized portion of the liver.
- **GPT-4o:** The liver appears normal in size and shape with a smooth capsule. The parenchymal echotexture is homogeneous with no obvious focal lesions. No intrahepatic or extrahepatic bile duct dilation is noted. The gallbladder is not clearly visualized in this image. No ascites or other fluid collections are present. Adjacent structures are not well visualized for further evaluation.
- **Gemini-1.5-Pro:** The liver appears normal in size with a smooth contour. The parenchymal echotexture is homogeneous with normal echogenicity. No focal lesions such as masses, cysts, or calcifications are identified. The intrahepatic bile ducts are not dilated. The portal venous structures appear normal.
- **Gemini-2.0-Pro-Exp:** The liver appears normal in size with a smooth capsule. The parenchymal echotexture is homogeneous with normal echogenicity. No focal lesions are identified. The intrahepatic bile ducts are not dilated. The portal venous structures appear normal where visualized.
- **Gemini-2.5-Pro-Preview:** The liver appears normal in size with a smooth capsule. The parenchymal echotexture is homogeneous with normal echogenicity. No focal lesions such as masses, cysts, or calcifications are identified. The intrahepatic bile ducts are not dilated. The portal venous structures appear normal where visualized. No perihepatic fluid collection is seen. The gallbladder and other adjacent structures are not well visualized in this limited image. Overall impression: Normal liver parenchyma without evidence of focal lesions or biliary dilation.
- **Claude-3.7-Sonnet:** The liver demonstrates normal size and contour with a smooth capsule. The parenchymal echotexture appears homogeneous with mildly increased echogenicity, suggesting possible early fatty infiltration. No focal lesions, masses, or cysts are identified. The intrahepatic biliary tree is not dilated. Portal venous structures appear normal where visualized. No perihepatic fluid collection is seen. Adjacent structures are not well visualized in this limited view.
- **Qwen-Max:** The liver appears normal in size with a smooth contour. The parenchymal echotexture is homogeneous with normal echogenicity. No focal lesions such as masses, cysts, or calcifications are identified. The intrahepatic bile ducts are not dilated. The portal venous structures appear normal. No perihepatic fluid collection is observed. The visualized portions of adjacent structures appear unremarkable. Overall, the liver appears sonographically normal based on this limited view.
- **Dolphin-V1:** The liver morphology is full with a smooth capsule. The parenchymal echotexture is fine and diffusely increased. Visualization of the portal venous system is suboptimal. Intrahepatic and extrahepatic bile ducts are not dilated. The main portal vein diameter is within normal limits. No focal lesions are identified.

1598 To provide deeper insights into model performance on medical imaging tasks, we conduct a comprehensive
 1599 error analysis of models across four critical ultrasound image analysis tasks: measurement, classification,
 1600 segmentation, and report generation. This analysis reveals distinct error patterns and task-specific challenges
 1601 that inform future model improvements.
 1602

1603 **Numerical Regression Task Analysis** Among 101 total responses, the most significant challenge is the
 1604 prevalence of **descriptive responses instead of numerical values** (53.47%). The model frequently generates
 1605 interpretative text such as “The principal anatomical element visualized here is unequivocally the fetus
 1606 head” rather than the expected numerical measurement (e.g., 291.4mm). This pattern suggests fundamental
 1607 misunderstanding of task requirements, where the model interprets the task as image content identification
 1608 rather than quantitative measurement.

1609 Format violations constitute 1.98% of responses, where models provide numerical values with units (e.g.,
 1610 “113.6 mm”) despite explicit formatting constraints. Notably, 43.56% of responses follow the correct
 1611 numerical format, though accuracy assessment requires comparison with ground truth values. The high rate
 1612 of descriptive responses indicates that current vision-language models struggle with the transition from visual
 1613 analysis to precise quantitative output.

1614
 1615 **Classification Task Performance** Classification tasks demonstrate superior format compliance compared
 1616 to measurement tasks, with 75.66% of responses providing valid option selections from 152 total responses.
 1617 However, two distinct error patterns emerge: **explanatory responses** (5.92%) where models provide justifica-
 1618 tions rather than selections (e.g., “There is no definitive view of the fetal abdomen or pelvis to determine fetal
 1619 position”), and **format violations** (18.42%) containing additional descriptive content alongside valid options.

1620 The tendency toward explanatory responses reveals an interesting model behavior where excessive caution
 1621 leads to task avoidance rather than best-effort selection from available options. This suggests that models
 1622 may benefit from more explicit instructions emphasizing the requirement for definitive option selection even
 1623 under uncertainty.

1624
 1625 **Segmentation and Localization Analysis** Segmentation tasks, requiring spatial reasoning for anatomical
 1626 structure localization, show moderate success with 66% valid position responses from 500 total responses.
 1627 The primary error categories include **invalid position terminology** (27.80%) with responses like “Not visible.”
 1628 or “Upper right.” that contain punctuation or non-standard terms, and **complete task deviation** (6.20%)
 1629 where models provide structural descriptions instead of positional information.

1630 **Case Study Examples:** Analysis of specific segmentation cases reveals distinct model behaviors. In thyroid
 1631 lesion localization tasks, while Gemini-2.5-Pro and GPT-4o consistently provide concise responses (“center”),
 1632 Claude-3.7-Sonnet exhibits significant format violations. For instance, when tasked with identifying tumor
 1633 location in breast ultrasound images, Claude generated extensive explanatory text:

1634 *“This image appears to be an ultrasound showing tissue layers with varying echogenicity...
 1635 I cannot identify a clear, definitive lesion... For proper medical diagnosis, this ultrasound
 1636 should be evaluated by a qualified radiologist...”*

1637 Such responses, while demonstrating medical awareness, completely violate the specified output format
 1638 requiring only location terms. This pattern suggests that Claude prioritizes safety disclaimers over task
 1639 compliance in medical contexts.

1641 Additionally, a concerning pattern emerges where multiple models consistently respond “center” regardless
 1642 of actual lesion position, as evidenced by reference bounding boxes indicating lesions at coordinates [0.6,
 1643 0.247] and [0.595, 0.308]. This suggests potential spatial reasoning limitations or default response bias that
 1644 could compromise clinical utility.

1645 The relatively high success rate in spatial localization compared to numerical measurement suggests that
1646 discrete spatial reasoning may be more accessible to current vision-language architectures than continuous
1647 numerical estimation.

1648

1649 **Report Generation Excellence** Report generation tasks achieve the highest success rate (98%) among all
1650 evaluated tasks, with only 2% exhibiting structural misidentification and 1% showing false findings. The
1651 rare but critical errors include anatomical misidentification (“Top view of fetus head and thorax” for fetal
1652 head ultrasound) and false pathological findings (“Aneuploid fetus with abnormal facial features”). While
1653 infrequent, such errors carry significant clinical implications, potentially leading to unnecessary medical
1654 interventions or patient anxiety.

1655

1656 **Cross-Task Error Pattern Analysis** Task difficulty ranking from most to least challenging reveals: measure-
1657 ment (43.56% success) > segmentation (66% success) > classification (75.66% success) > report
1658 generation (98% success). This hierarchy reflects the increasing complexity of transitioning from free-form
1659 text generation to structured, constrained outputs requiring precise adherence to format specifications.

1660 Common error patterns across tasks include: (1) **descriptive language substitution**, most prominent in
1661 measurement tasks where models default to interpretative text rather than required numerical values; (2)
1662 **format non-compliance**, prevalent across classification and segmentation tasks despite clear formatting
1663 instructions; and (3) **task misunderstanding**, where models completely misinterpret task objectives, such as
1664 treating localization as structure identification.

1665

1666 **Implications for Medical AI Development** These findings highlight critical considerations for deploying
1667 vision-language models in medical imaging applications. The inverse relationship between task constraint and
1668 model performance suggests that current architectures excel at unconstrained text generation but struggle with
1669 precise, structured outputs essential for clinical decision-making. Future developments should prioritize: (1)
1670 enhanced instruction following capabilities for constrained output generation, (2) domain-specific fine-tuning
1671 on medical imaging tasks emphasizing numerical precision, and (3) robust validation mechanisms to detect
1672 and prevent false findings in clinical applications.

1673 The analysis underscores that while large vision-language models show promise for medical imaging applica-
1674 tions, careful task-specific optimization and human oversight remain essential, particularly for quantitative
1675 measurements and diagnostic assessments where precision directly impacts patient care.

1676

1677

1678

1679

1680

1681

1682

1683

1684

1685

1686

1687

1688

1689

1690

1691

1692 **D PROMPT FOR TASKS**
1693

1694

1695

1696

1697

1698

1699

1700

1701 **Prompt Template used for fetal view classification (dataset 10)**

1702 You are a radiologist analyzing a fetal ultrasound image.

1703 Your task is to determine the fetal presentation and orientation based on the provided ultrasound image. Specifically, identify whether the fetal head is down(hd) or up(hu). Additionally, determine if the fetal back is primarily oriented towards the ultrasound probe (vb) or towards the ultrasound probe (vf). Choose the single best option from the options below that accurately combines these findings.

1704
1705 options: 'hdvb', 'hdvf', 'huvb', 'huvf'

1706
1707 Output format: only the exact text of the chosen option from the list above. Do not include any
1708 introductory phrases, explanations, numbering, or formatting.

1709

1710

1711
1712 Output format: only the exact text of the chosen option from the list above. Do not include any
1713 introductory phrases, explanations, numbering, or formatting.

1714

1715

1716

1717

1718

1719

1720

1721

1722

1723

1724 **Prompt Template used for heart view classification (dataset 18)**

1725

1726 You are a radiologist or cardiologist specializing in echocardiography, analyzing an apical view
1727 ultrasound image of the human heart.

1728 Your task is to accurately identify the specific apical view presented in the provided echocardiogram
1729 image. Carefully examine the cardiac structures visible. Determine if the image displays primarily the
1730 left ventricle and left atrium only (indicative of a 2-Chamber view, 2CH), or if it clearly shows all four
1731 chambers: the left ventricle, right ventricle, left atrium, and right atrium (indicative of a 4-Chamber
1732 view, 4CH). Choose the single best option from the list below that correctly identifies the view.

1733
1734 options: 2CH, 4CH

1735

1736 Output format: only the exact text of the chosen option from the list above. Do not include any
1737 introductory phrases, explanations, numbering, or formatting.

1738

Prompt Template used for (KL) grading (dataset 28)

You are a radiologist analyzing an ultrasound image of left/right knee.

Your task is to assess the severity of osteoarthritis (OA) using the established Kellgren-Lawrence (KL) grading system. Kellgren-Lawrence (KL) Grade Mapping to Options:

- 'No OA': Corresponds to KL Grade 0 (No radiographic features of OA).
- 'Questionable OA': Corresponds to KL Grade 1 (Doubtful JSN and possible minute osteophytes).
- 'Mild OA': Corresponds to KL Grade 2 (Definite osteophytes and possible JSN).
- 'Moderate OA': Corresponds to KL Grade 3 (Moderate multiple osteophytes, definite JSN, some sclerosis, possible deformity).
- 'Severe OA': Corresponds to KL Grade 4 (Large osteophytes, marked JSN, severe sclerosis, definite deformity).
- 'Total joint replacement': Indicates the presence of knee arthroplasty components (prostheses), which replaces the native joint structures evaluated by the KL scale.

Choose the single best option from the following list that accurately describes the image.

options: 'Mild OA', 'Moderate OA', 'No OA', 'Questionable OA', 'Severe OA', 'Total joint replacement'

Output format: only the exact text of the chosen option from the list above. Do not include any introductory phrases, explanations, numbering, or formatting.

Prompt Template used for BI-RADS classification (dataset 40)

You are a radiologist analyzing a breast ultrasound image.

Your task is to synthesize the sonographic characteristics of any identified lesions (or lack thereof) into a final ACR BI-RADS (Breast Imaging Reporting and Data System) assessment category.

BI-RADS Ultrasound Assessment Category Definitions:

- '2' (Benign): Findings are definitively benign (e.g., simple cysts, intramammary lymph nodes, stable surgical implants/changes). 0% likelihood of malignancy. Requires routine screening follow-up.
- '3' (Probably Benign): Findings have characteristic benign features but are not definitively benign (e.g., presumed fibroadenoma, complicated cyst). Very low likelihood of malignancy ($\leq 2\%$). Short-interval (e.g., 6-month) follow-up is typically recommended.
- '4A' (Low Suspicion for Malignancy): Findings warrant biopsy but have a low probability of malignancy ($\leq 2\%$ to $\leq 10\%$).
- '4B' (Moderate Suspicion for Malignancy): Findings warrant biopsy with an intermediate probability of malignancy ($\leq 10\%$ to $\geq 50\%$).
- '4C' (High Suspicion for Malignancy): Findings warrant biopsy with a high probability of malignancy ($\geq 50\%$ to $\geq 95\%$), without the classic features of Category 5.
- '5' (Highly Suggestive of Malignancy): Findings have classic malignant features (e.g., irregular spiculated mass). Very high probability of malignancy ($\geq 95\%$). Biopsy is required, and definitive action should be taken regardless of pathology results if discordant.

Choose the single most appropriate BI-RADS assessment category from the options below.

options: ['2', '3', '4A', '4B', '4C', '5']

Output format: only the exact text of the chosen option from the list above. Do not include any introductory phrases, explanations, numbering, or formatting.

Prompt Template used for fetal abdomen (dataset 50)

You are a radiologist analyzing an ultrasound image of fetal abdomen.

Your task is to determine if the presented cross-sectional view of the fetal abdomen is technically adequate for performing an accurate Abdominal Circumference (AC) measurement according to standard obstetric guidelines. Identify the specific anatomical plane shown for the fetal abdomen. Determine if this plane meets the criteria for an optimal AC measurement (correct landmarks visible, proper transverse orientation) or if it is suboptimal (incorrect plane, missing landmarks, oblique/-foreshortened view, presence of interfering structures like kidneys). Choose the single best option describing the plane's suitability for AC measurement.

options: 'none', 'optimal', 'suboptimal'

Output format: only the exact text of the chosen option from the list above. Do not include any introductory phrases, explanations, numbering, or formatting.

1833 Prompt Template used for breast classification

1834

1835 You are a radiologist analyzing a breast ultrasound image.

1836

1837 Your task is carefully examine the provided breast ultrasound image, evaluate any identified lesions or

1838 abnormalities based on key sonographic characteristics (including shape, orientation, margin, echo

1839 pattern, posterior acoustic features, and associated features), synthesize these features to form an

1840 overall impression about the likelihood of malignancy, and then choose the single best option from

1841 the following list that accurately summarizes this assessment.

1842

1843 options: (normal), benign, malignant

1844

1845 Output format: only the exact text of the chosen option from the list above. Do not include any

1846 introductory phrases, explanations, numbering, or formatting.

1847

1848 Prompt Template used for thyroid classification

1849

1850 You are a radiologist specializing in head and neck or endocrine imaging, analyzing an ultrasound

1851 image of the thyroid gland.

1852

1853 Your task is to carefully examine the provided thyroid ultrasound image, evaluate the overall thyroid

1854 gland parenchyma (echogenicity, texture, vascularity), identify any focal nodules, assess the specific

1855 sonographic features of any nodules found (including composition, echogenicity, shape, margin,

1856 and echogenic foci), synthesize these findings to determine if the gland appears normal, contains

1857 benign-appearing findings, or contains findings suspicious for malignancy, and then choose the single

1858 best option from the following list that accurately summarizes this assessment.

1859

1860 options: (normal thyroid), benign, malignant

1861

1862 Output format: only the exact text of the chosen option from the list above. Do not include any

1863 introductory phrases, explanations, numbering, or formatting.

1864

1865 Prompt Template used for skin cancer classification (dataset 25)

1866

1867 You are a radiologist analyzing an ultrasound image of skin.

1868

1869 Your task is to carefully examine the provided skin ultrasound image, evaluate the identified lesion

1870 or abnormality based on key sonographic characteristics (including its location within skin layers,

1871 echogenicity, internal echo texture, shape, margins, size/depth, posterior acoustic phenomena, and

1872 vascularity assessed with Doppler), synthesize these features to form an overall impression regarding

1873 the likelihood of malignancy, and then choose the single best option from the following list that

1874 summarizes this assessment.

1875

1876 options: benign, malignant

1877

1878 Output format: only the exact text of the chosen option from the list above. Do not include any

1879 introductory phrases, explanations, numbering, or formatting.

1880
1881 Prompt Template used for pancreas cancer classification (dataset 42)
1882
1883 You are a radiologist analyzing an ultrasound image of the pancreas.
1884
1885 Your task is to carefully examine the provided ultrasound image of the pancreas, evaluate the gland's
1886 echotexture, size, margins, and the pancreatic duct diameter, identify any focal lesions or masses
1887 (noting their echogenicity, margins, size, and vascularity if Doppler is available), assess for associated
1888 findings such as ductal dilation (including potential "double duct" sign), vascular involvement
1889 (encasement/thrombosis), regional lymphadenopathy, or fluid collections, synthesize these findings to
1890 determine if there is evidence suspicious for primary pancreatic cancer versus other findings, and then
1891 choose the single best option from the following list that summarizes this assessment.
1892
1893 options: non-pancreas cancer, pancreas cancer

1894
1895 Output format: only the exact text of the chosen option from the list above. Do not include any
1896 introductory phrases, explanations, numbering, or formatting.

1896
1897
1898
1899
1900
1901
1902
1903
1904
1905
1906
1907
1908
1909
1910 Prompt Template used for PCOS classification (dataset 74)
1911
1912 You are a radiologist analyzing an ultrasound image obtained during a pelvic examination, potentially
1913 as part of an evaluation for Polycystic Ovary Syndrome (PCOS).
1914
1915 Your task is to evaluate the overall appearance of the anatomical structures presented in the ultrasound
1916 image (primarily focusing on the ovaries and potentially the uterus). Consider sonographic features
1917 such as ovarian size, morphology, follicle count and distribution, stromal echogenicity, as well as
1918 any other findings that might indicate pathology. Based on this assessment, determine if the image
1919 appears generally normal or if it displays features suggestive of an abnormality (which could include
1920 findings consistent with PCOS or other conditions). Choose the single best option from the following
1921 list that accurately describes this overall impression.
1922
1923 options: 'Appears abnormal', 'Appears normal'

1924
1925 Output format: only the exact text of the chosen option from the list above. Do not include any
1926 introductory phrases, explanations, numbering, or formatting.

1927
1928
1929
1930
1931
1932
1933
1934
1935
1936
1937
1938
1939
1940
1941
1942
1943
Prompt Template used for PCOS classification (dataset 74)

You are a radiologist analyzing an ultrasound image obtained during a pelvic examination. Crucially, assume this specific image has already been determined to show some form of abnormality. Your focus now is on the nature of that abnormality.

Your task is to specifically assess whether the abnormality present in this ultrasound image includes clear sonographic evidence consistent with a polycystic ovary. Evaluate the visualized ovarian structures, paying close attention to features commonly associated with PCOS, such as: increased number of follicles, peripheral distribution of follicles, increased ovarian volume, increased stromal echogenicity or volume. Based on whether these specific PCOS-related sonographic features are identifiable within the overall abnormal appearance, specifies whether the ultrasound image shows evidence/ visibility of a polycystic ovary or not. Choose the single best option from the following list.

options: 'Not-visible', 'Visible'

Output format: only the exact text of the chosen option from the list above. Do not include any introductory phrases, explanations, numbering, or formatting.

2021
2022

Prompt Template used for fetal (dataset 03)

You are a radiologist analyzing a single ultrasound image acquired during a fetal examination.

Your task is to carefully examine the provided image, identify the primary anatomical structure or region being visualized, and determine the most appropriate description based on the standard imaging planes used in fetal ultrasound. Choose the single best option from the following list that accurately describes the main subject shown in the image.

options: 'fetal abdomen', 'fetal femur', 'fetal brain', 'fetal thorax', 'maternal cervix', 'other'

Output format: only the exact text of the chosen option from the list above. Do not include any introductory phrases, explanations, numbering, or formatting.

2029

2030

2031

2032

2033

2034

2035

2036

2037

Prompt Template used for thyroid plane classification (dataset 37)

You are a radiologist with expertise in interpreting neck and thyroid ultrasound images. You are presented with a single B-mode ultrasound image focused on the thyroid gland and adjacent neck structures.

Your task is to identify the Cardinal Anatomical Plane depicted in the provided ultrasound image. Choose the single best option from the following list that accurately describes the image.

options: 'Axial/Transverse Plane', 'Coronal Plane', 'Sagittal Plane'

Output format: only the exact text of the chosen option from the list above. Do not include any introductory phrases, explanations, numbering, or formatting.

2043

2044

2045

2046

2047

2048

2049

2050

2051

2052

2053

Prompt Template used for fetal (dataset 53)

You are a radiologist analyzing a single B-mode ultrasound image obtained during a fetal assessment.

Your task is to carefully examine the provided ultrasound image frame to identify the presence or absence of two specific anatomical landmarks: the fetal head and the maternal symphysis pubis. Based on this identification, classify the frame's content by choosing the single best option from the following list that accurately describes which of these landmarks are visible. Choose the single best option from the following list that accurately describes the frame's content.

options: 'None', 'OnlyFetalHead', 'OnlySymphysisPubis', 'SymphysisPubis+FetalHead'

Output prompt: only the exact text of the chosen option from the list above. Do not include any introductory phrases, explanations, numbering, or other formatting.

2054

2055

2056

2057

2058

2059

2060

2061

2062

2063

2064

2065

2066

2067

Prompt Template used for carotid classification (dataset 69)

You are a radiologist analyzing an ultrasound image depicting a portion of the carotid arterial system in the neck.

Your task is to carefully examine the provided ultrasound image, analyzing anatomical landmarks, vessel morphology, and its position relative to other neck structures, to identify the primary carotid artery segment shown. Choose the single best option from the following list that accurately describes the main vessel visualized in the frame's content. Assume 'left carotid' and 'right carotid' refer generally to the common or internal carotid artery on that respective side, while 'external carotid' refers specifically to the external carotid artery branch. Choose the single best option from the following list that accurately describes the image.

options: 'external carotid', 'left carotid', 'right carotid'

Output prompt: only the exact text of the chosen option from the list above. Do not include any introductory phrases, explanations, numbering, or other formatting.

Prompt Template used for anatomy classification

You are an expert specialized in analyzing medical ultrasound images. You are provided with a single ultrasound image frame, which could depict various parts of the human body.

Your task is to analyze the provided ultrasound image and identify the primary anatomical region or organ system being visualized. Choose the single best option from the following list that most accurately represents this primary anatomical subject.

options: 'fetal', 'thyroid', 'heart', 'lung', 'liver', 'carotid', 'kidney', 'prostate', 'breast', 'other'

Output prompt: only the exact text of the chosen option from the list above. Do not include any introductory phrases, explanations, numbering, or other formatting.

2115
2116 Prompt Template used for knee classification
2117
21182119 You are a radiologist analyzing an ultrasound image of knee.
2120
2121 Your task is to classify the specific anatomical view, laterality (left/right), orientation, and any specific
2122 imaging technique or patient positioning shown in the image:
2123

- 2124 • 'left anterior suprapatellar longitudinal': Image of the left knee, taken from the front (anterior), just above the kneecap (suprapatellar), with the ultrasound probe oriented along the long axis of the thigh/patellar tendon. Standard B-mode imaging.
2125
- 2126 • 'left anterior suprapatellar longitudinal with power Doppler': Same view as above (left, anterior suprapatellar, longitudinal), but with Power Doppler mode activated, typically used to assess blood flow or inflammation.
2127
- 2128 • 'left anterior suprapatellar transverse in 30 degrees flexion': Image of the left knee, from the front (anterior), above the kneecap (suprapatellar), with the probe oriented across (transverse) the thigh, and the knee bent at approximately 30 degrees.
2129
- 2130 • 'left anterior suprapatellar transverse in maximal flexion': Same view as above (left, anterior suprapatellar, transverse), but with the knee bent as much as possible (maximal flexion).
2131
- 2132 • 'left lateral longitudinal': Image of the outer side (lateral) of the left knee, with the probe oriented along the long axis of the structures (e.g., LCL, IT band).
2133
- 2134 • 'left medial longitudinal': Image of the inner side (medial) of the left knee, with the probe oriented along the long axis of the structures (e.g., MCL, medial meniscus).
2135
- 2136 • 'left posterior medial transverse': Image of the back, inner corner (posterior medial) of the left knee, with the probe oriented across (transverse) the structures (often used for Baker's cysts).
2137
- 2138 • 'right anterior suprapatellar longitudinal': Image of the right knee, taken from the front (anterior), just above the kneecap (suprapatellar), with the ultrasound probe oriented along the long axis of the thigh/patellar tendon. Standard B-mode imaging.
2139
- 2140 • 'right anterior suprapatellar longitudinal with power Doppler': Same view as above (right, anterior suprapatellar, longitudinal), but with Power Doppler mode activated.
2141
- 2142 • 'right anterior suprapatellar transverse in 30 degrees flexion': Image of the right knee, from the front (anterior), above the kneecap (suprapatellar), with the probe oriented across (transverse) the thigh, and the knee bent at approximately 30 degrees.
2143
- 2144 • 'right anterior suprapatellar transverse in maximal flexion': Same view as above (right, anterior suprapatellar, transverse), but with the knee bent as much as possible (maximal flexion).
2145
- 2146 • 'right lateral longitudinal': Image of the outer side (lateral) of the right knee, with the probe oriented along the long axis of the structures.
2147
- 2148 • 'right medial longitudinal': Image of the inner side (medial) of the right knee, with the probe oriented along the long axis of the structures.
2149
- 2150 • 'right posterior medial transverse': Image of the back, inner corner (posterior medial) of the right knee, with the probe oriented across (transverse) the structures.
2151

2152 Choose the single best option from the following list that accurately describes the image.
2153
21542155 Options: 'left anterior suprapatellar longitudinal', 'left anterior suprapatellar longitudinal with power
2156 Doppler', 'left anterior suprapatellar transverse in 30 degrees flexion', 'left anterior suprapatellar
2157 transverse in maximal flexion', 'left lateral longitudinal', 'left medial longitudinal', 'left posterior
2158 medial transverse', 'right anterior suprapatellar longitudinal', 'right anterior suprapatellar longitudinal
2159 with power Doppler', 'right anterior suprapatellar transverse in 30 degrees flexion', 'right anterior
2160 suprapatellar transverse in maximal flexion', 'right lateral longitudinal', 'right medial longitudinal',
2161 'right posterior medial transverse'2162 Output prompt: only the exact text of the chosen option from the list above. Do not include any
2163 introductory phrases, explanations, numbering, or other formatting.

2162
2163

Prompt Template used for lesion detection

2164
2165

You are a radiologist analyzing an ultrasound image of thyroid.

2166
2167

Your task is to identify the primary location of any visible lesion(s) relative to the boundaries of the displayed image. Consider the lesion's center location or most prominent area when deciding. Choose the single option from the list below that best describes this location, even if the fit is approximate.

2168
2169

Choose the single most appropriate location from the following list:

2170
2171

- upper left
- upper center
- upper right
- middle left
- center
- middle right
- lower left
- lower center
- lower right
- not visible

2172
2173

Output format: only one or two word(s) representing the chosen location. No additional text or

2174
2175

formatting is allowed.

2176
2177

2178
2179

2180
2181

2182
2183

2184

Output format: only one or two word(s) representing the chosen location. No additional text or

2185
2186

2187

2188

2189

2190

2191

2192

2193

2194

2195

2196

2197

2198

2199

2200

2201

2202

2203

2204

2205

2206

2207

2208

2209
2210 Prompt Template used for organ detection
2211
2212
2213 You are a radiologist analyzing an ultrasound image of abdominal.
2214
2215 Your task is to determine the primary location, relative to the image boundaries, for each visible
2216 structure listed in liver.
2217
2218

- Consider the structure's center or most prominent area when deciding its location.
- Choose the single option from the list below that best describes the location, even if the fit is
2219 approximate.

2220 Location Options:
2221

- upper left
- upper center
- upper right
- middle left
- center
- middle right
- lower left
- lower center
- lower right
- not visible

2222
2223
2224
2225
2226
2227
2228
2229
2230
2231
2232
2233
2234
2235 Output format: only one or two word(s) representing the chosen location. No additional text or
2236 formatting is allowed.
2237
2238
2239
2240
2241
2242
2243
2244
2245
2246
2247
2248
2249
2250
2251
2252
2253
2254
2255

2256
2257

Prompt Template used for keypoint detection

2258
2259

You are a radiologist analyzing an ultrasound image of the heart.

2260
2261
2262
2263
2264

Your task is to determine the top inner point of the aortic valve.

- Consider the structure's center or most prominent area when deciding its location.
- Choose the single option from the list below that best describes the location, even if the fit is approximate.

2265
2266
2267
2268
2269
2270
2271
2272
2273
2274
2275
2276
2277
2278
2279

Location Options:

- upper left
- upper center
- upper right
- middle left
- center
- middle right
- lower left
- lower center
- lower right
- not visible

2280
2281
2282

Output format: only one or two word(s) representing the chosen location. No additional text or formatting is allowed.

2283
2284
2285
2286
2287

Prompt Template used for caption generation

2288
2289
2290
2291
2292
2293

You are a radiologist analyzing an ultrasound image focused on the {anatomy_location}.

Your task is to generate a concise and informative caption that accurately describes the key anatomical structures and any significant findings visible in the provided ultrasound image.

2294
2295
2296
2297

Output format: A single string constituting the image caption. Output only the generated caption text itself. Do not include any introductory phrases (like Caption:), labels, explanations, or additional formatting.

2298
2299
2300
2301
2302

Examples:

- Example1: Thyroid nodule in the right lobe. TI-RADS level 3, Benign.
- Example2: Thyroid nodule in the left lobe. TI-RADS level 3, Benign.
- Example3: Thyroid nodule in the right lobe. TI-RADS level 4, Benign.

2303
2304

Prompt Template used for report generation

2305
2306

You are a radiologist analyzing an ultrasound image focused on the {anatomy_location}.

2307
2308
2309
2310
2311
2312

Your task is generate a concise and informative radiological report based strictly on the visual findings within the provided image. Your report should describe the primary organ's appearance (size, shape, borders/capsule), its parenchymal echotexture (e.g., homogeneous, heterogeneous, echogenicity relative to reference structures), and identify any visible abnormalities (e.g., masses, cysts, fluid collections, calcifications, ductal dilation). Comment on relevant adjacent structures if visualized. Use standard radiological terminology.

2313
2314

Output format: Strings, that is your report.

2315
2316
2317
2318
2319
2320
2321
2322

Example: The liver morphology is full with a smooth capsule. The parenchymal echotexture is fine and diffusely increased. Visualization of the portal venous system is suboptimal. Intrahepatic and extrahepatic bile ducts are not dilated. The main portal vein diameter is within normal limits. The gallbladder is normal in size and shape. The wall is smooth and not thickened. No obvious abnormal echoes are seen within the lumen. The pancreas is normal in size and shape with homogeneous parenchymal echotexture. The pancreatic duct is not dilated. No definite space-occupying lesion is seen within the pancreas. The spleen is normal in size and shape with homogeneous parenchymal echotexture. No obvious space-occupying lesion is seen within the spleen.

2323
2324
2325
2326
2327
2328
2329
2330
2331
2332
2333
2334
2335
2336
2337
2338
2339
2340
2341
2342
2343
2344
2345
2346
2347
2348
2349

E DATASET DETAILS AND LICENSE

Table 7: Summary of Annotated Datasets Used in U2-BENCH

Dataset	Anatomy	Clinical scenarios	Task	Case	License
FETAL PLANES DB (Burgos-Artizzu et al., 2020)	Fetal abdomen Fetal brain Fetal femur Fetal thorax Maternal cervix other	Fetal standard plane identification	VRA	137	CCA 4.0I
DDTI (Pedraza et al., 2015)	thyroid	Thyroid nodule identification Thyroid nodule localisation	VRA LL	110	-
The Open Kidney US Dataset (Singla et al., 2023)	kidney	Kidney detection Kidney Diag view identification	VRA OD	110	CC BY-NC-SA
FPUS23 (Prabakaran et al., 2023)	Fetal abdomen Fetal arm Fetal head Fetal legs	Fetal diagnostic planes identification Fetal US report generation	VRA RP	752	MIT
Echogenic (Da Correggio et al., 2023)	Fetal abdomen	Fetal abdominal organ detection	OD	102	CCA 4.0
FALLMUD (FALL-MUD)	Crural muscles	Muscle detection	OD	100	-
Micro-US Prostate Segmentation Dataset (Shao & Brisbane, 2024)	Prostate	Prostate localisation Prostate Diag view identification	VRA LL	110	CCA 4.0I
CAMUS (Leclerc et al., 2019)	Heart ED Heart ES Heart 2CH Heart 4CH	Heart ejection fraction estimation Heart atrium and ventricle localisation	VRA OD CVE	316	CC BY-NC-SA 4.0
Breast Lesion Detection in US Videos (Lin et al., 2022)	Breast benign Breast malignant	Breast lesion classification	Diag	171	-

Continued on next page

(Continued) Table 7

2397	Dataset	Anatomy	Clinical scenarios	Task	Case	License
2398	Breast US Images Dataset (Al-Dhabyani et al., 2020)	Breast	Breast cancer level classification Breast tumour localisation Brest Diag view identification	Diag VRA LL	210	CC0: PD
2400	Dermatologic Ultrasound Images for classification (Laverde Saad et al., 2021)	Skin	Skin tumor level classification	Diag	100	-
2401	Polycystic Ovary Ultrasound Images Dataset (Wisesty et al., 2018)	Ovary	Polycystic Ovary Syndrome localisation	VRA	10	CC0: PDD
2402	CUBS (Meiburger et al., 2021)	Carotid	Carotid thickness estimation Carotid detection Catotid Diag view identification	VRA OD CVE	681	CCA 4.0I
2403	Knee US dataset in a population-based cohort (Novin et al., 2023)	Knee	Knee US KL and pain grad classification Knee Diag view identification Knee lesion localisation	Diag VRA OD	326	CC0 1.0
2404	HC18 (van den Heuvel et al., 2018)	Fetal head	Fetal head circumference estimation Fetal head detection	OD CVE	202	CCA 4.0I
2405	KFGNet (NeuronXJTU & palkia1998, 2023)	Thyroid	Thyroid nodule level classification Thyroid nodule localisation	Diag LL	206	-
2406	Thyroid (Krönke et al., 2022)	Thyroid Left Thyroid right	Thyroid Diag view identification	VRA	563	CC BY
2407	GDPHSYSUCC (Mo et al., 2022)	Breast	Breast lesion classification	Diag	109	-
2408	LEPset (Li et al., 2023b)	Pancreas	Pancreatic cancer classification	Diag	101	CCA 4.0I

Continued on next page

(Continued) Table 7

Dataset	Anatomy	Clinical scenarios	Task	Case	License
COVID-BLUES (Wiedemann et al., 2025)	Lung	COVID-19 level classification Lung US caption generation Lung Diag view identification	Diag VRA CG	318	ANN 4.0 I
Ultrasound Guided Regional Anesthesia (Tyagi et al., 2024)	Brachial plexus	Brachial plexus detection	OD	179	Non-commerical
Unity Imaging Collaborative (Shun-Shin, 2023)	Cardiac	Cardiac Keypoint Detection	KD	500	CCANN 4.0 I
C-TRUS Dataset (Leenings et al., 2025)	Colon	Colon wall detection	OD	166	-
ACOUSLIC-AI (Sappia, 2024)	Fetal abdominal	Fetal abdominal circumference estimation Fetal abdominal OD	VRA OD CVE	310	CCANCSA 4.0I
PSFHS (Bai, 2024)	Fetal head Fetal pubic symphysis	Fetal head detection Fetal pubic symphysis detection	OD	100	CCA 4.0I
JNU-IFM (Lu et al., 2022)	Fetal head Fetal pubic symphysis	Fetal view identification Fetal head detection Fetal pubic symphysis detection	VRA OD	202	CC BY 4.0
Dataset of B-mode fatty liver US images (Byra et al., 2018)	Liver	Liver steatosis classification Liver fat value estimation Liver Diag view identification	Diag VRA CVE	222	CCA 4.0I
African Fetal Standard Plane (Sendra-Balcells et al., 2023)	Fetal abdomen Fetal brain Fetal femur Fetal thorax	Fetal standard plane identification	VRA	10	CCA 4.0I
BrEaST (Pawłowska et al., 2024)	Breast	Breast LL	LL	100	CC BY 4.0
Ultrasound Breast Images for Breast Cancer (Sairam, 2020)	Breast	Breast cancer classification	Diag	100	CC0: PD

Continued on next page

(Continued) Table 7

Dataset	Anatomy	Clinical scenarios	Task	Case	License
US simulation and segmentation (Vitale et al., 2020)	Abdominal	Abdominal OD	OD	100	-
Carotid Artery Ultrasound and Color Doppler (Pahuni Choudhary, 2023)	External carotid left carotid right carotid	Carotid Diag view identification	VRA	100	Apache 2.0
AUITD (Maroua, 2020)	Thyroid	Thyroid lesion classification	Diag	100	-
Auto-PCOS classification (Maroua, 2020)	Ovary	Polycystic Ovary Syndrome classification Polycystic Diag view identification	Diag VRA	218	CCA 4.0I
Auto-PCOS classification (Maroua, 2020)	Ovary	Polycystic Ovary Syndrome classification	Diag	100	CC BY 4.0

2514 E.1 SUMMARY OF DATASET LICENSING TERMS

2515 The datasets included in **U2-BENCH** span a range of open and restricted licenses. For clarity, we summarise
2516 the licensing terms appearing in Table 7.

- 2518 • **CC0 / Public Domain (PD, PDD):** Fully open; free use, modification, and redistribution without
2519 attribution, including commercial use.
- 2520 • **CC BY / CC BY 4.0 / CCA 4.0I:** Free use with attribution; permits modification and redistribution.
- 2521 • **CC BY-NC-SA / CC BY-NC-SA 4.0 / variants written as ANN 4.0 I, CCANN 4.0 I, CCANCSA
2522 4.0I:** Non-commercial use only; derivatives must adopt the same license.
- 2523 • **CC BY-NC-ND:** Attribution required; non-commercial; no derivatives permitted. Minor naming
2524 variations follow the dataset providers' release notes.
- 2525 • **MIT License:** Permissive license allowing free use, modification, and redistribution, including
2526 commercial applications.
- 2527 • **Apache 2.0:** Permissive license with an explicit patent grant.
- 2528 • **Non-commercial data use agreement:** Access provided strictly for non-commercial research;
2529 redistribution or reuse requires separate permission.
- 2530 • **Unspecified / “-”:** Publicly released datasets without an explicit license. Usage follows the terms
2531 communicated by the original authors.

2534 These variations reflect the diverse data-sharing practices in medical imaging. All usage within **U2-BENCH**
2535 complies with the terms of the original dataset providers.